MICRORNA-506-3P AS A DIFFERENTIATION AGENT FOR NEUROBLASTOMA

by

Michaela M. Sousares, B.S.

A thesis submitted to the Graduate Council of
Texas State University in partial fulfillment
of the requirements for the degree of
Master of Science
with a Major in Biochemistry
August 2017

Committee Members:

Liqin Du, Chair

L. Kevin Lewis

Karen A. Lewis

FAIR USE AND AUTHOR'S PERMISSION STATEMENT

Fair Use

Duplicate Permission

DEDICATION

To my parents, Jerry D. Sousares and Lisa K. Sousares, and my sisters,
Danielle R. Sousares and Adrienne E. Sousares.
This would not have been possible without your continued support.

ACKNOWLEDGEMENTS

I would like to thank my research advisor, Dr. Liqin Du, for providing me with the opportunity to work in her lab and for encouraging creativity. I would like to thank my committee members, Dr. L. Kevin Lewis and Dr. Karen A. Lewis for their advice and guidance throughout my thesis project and academic career. I would also like to thank my lab colleagues, Veronica R. Partridge, Geraldo Medrano, and Daniel Hernandez for their constant support and encouragement as we spent many days and nights in the lab, and for their friendships that I hope to carry for years to come. A special thanks to Dr. Zhenze Zhao for training me in the lab, providing answers for my constant questions, and being my primary source for troubleshooting, inspiration, contemplation, and more.

I would like to thank Dr. Robert J.C. McLean and Dr. Craig A. Damin for providing advice, encouragement, and a kind ear during my project.

My family members, Jerry D. Sousares, Lisa K. Sousares, Danielle R. Sousares, Adrienne E. Sousares, and my grandparents, Billy R. Blaylock and Caroline H. Blaylock supplied me with the love, support, and encouragement that allowed me to do my best in completing my project and academics. I would like to extend my gratitude towards Natasha N. Moye and Hina P. Patel for their constant love and friendship during my studies.

Finally, I'd like to thank Lance R. English for introducing me to research science, and for providing me with inspiration and encouragement throughout both my undergraduate and graduate degrees.

TABLE OF CONTENTS

LIST OF TABLES

Table **Page**

LIST OF FIGURES

Figure **Page**

LIST OF ABBREVIATIONS

Abbreviation	Description
ATRA	All-*Trans*-Retinoic Acid
DMEM	Dulbecco's Modified Eagle's Medium
DPBS	Dulbecco's Phosphate-Buffered Saline
GAP43	Growth Associated Protein 43
miRNA(s)	microRNA(s)
miR-506-3p	microRNA-506-3p
MYCN	N-Myc Proto-oncogene Protein
NO	Neurite Outgrowth
NSE	Neuron Specific Enolase
PBS	Phosphate Buffered Saline
SDS	Sodium Dodecyl Sulfate
SDS-PAGE	Sodium Dodecyl Sulfate Polyacrylamide Gel Electrophoresis
SEM	Standard Error of the Mean
TEMED	Tetramethylethylenediamine
TH	Tyrosine Hydroxylase
TRIS	Tris(hydroxymethyl)aminomethane

ABSTRACT

Neuroblastoma is the most common solid tumor cancer in infants less than 1 year of age, and the second most common extracranial cancer in children. Approximately 60% of the cases have already spread to the lymph nodes at diagnosis, where children with this disease typically do not live past 10 years of age. The high mortality rate of this cancer arises from the failure of neural crest cell precursors to differentiate, which inhibits the maturation of these cells, leaving immortal, infant malignancies. 13-*cis*-retionoic acid is currently used as the agent of choice for neuroblastoma, but exhibits a 50% recurrence of tumor cells, leaving the identification of new targets a crucial step in the elucidation of neuroblastoma.

MicroRNAs are small, noncoding RNAs, that regulate transcription and the expression of many genes. They perform posttranscriptional gene modification by translational suppression, mRNA degradation, or site-specific cleavage of mRNAs. The dysregulation of these molecules leads to tumor development and metastasis, along with chemoresistance and multidrug resistance. MicroRNA mimics are partially double-stranded RNAs designed to mimic the function of endogenous miRNAs, effectively increasing the level of cellular miRNAs. Recent studies have provided evidence for the use of miRNAs in the induction of differentiation of neuroblastoma cells, which induce malignant cells to mature and undergo apoptosis. More recently, a novel miRNA, miR-506-3p, was identified as a potent inducer of neuroblastoma cell differentiation by the

down-regulation of two target genes at the 3'UTR target site, suggesting this as an effective differentiation agent for neuroblastomal remission therapy.

The current study examined the effects of retinoic acid and miR-506-3p mimic, alone and in combination, on undifferentiated neuroblastoma cells. To approach this, techniques such as cell culture, forward and reverse transfection, neurite outgrowth assays, cell viability assays, cell proliferation assays, and Western Blot were used to quantify the differentiation-inducing effect of these treatments. For both ATRA and miR-506-3p mimic-treated cells with different genetic backgrounds, there were variations in responses. More cell lines responded to the miR-506-3p mimic, suggesting a more general effect than ATRA on neuroblastoma cell differentiation. For combined treatments, all experimental values were less than the predicted. In sum, the results provided here support the hypothesis that the miR-506-3p mimic may have a broader effect than ATRA on neuroblastoma cell differentiation, but no synergism can be reported for the response following combined treatments on neuroblastoma cell viability. However, an enhanced effect for the combined treatments was observed.

I. INTRODUCTION

1.1 Neuroblastoma

Neuroblastoma is a neoplasm of the sympathetic nervous system, where tumors can arise anywhere along nerve tissues in this system.[1] Tumors preferentially develop in the abdomen about 65% of the time, with half of these present in the adrenal gland.[1] Neuroblastomal tumors also develop in the neck, chest, and pelvis.[1] It is the most common solid tumor cancer in infants less than 1 year of age, and the second most common extracranial cancer in children.[1] Neuroblastoma makes up about 7% of all childhood cancers, with 700 new cases in the USA every year, in children under the age of 15.[1] The average age of diagnosis is 1-2 years old, but it has been detected in pre-birth by ultrasound.[2] Approximately 60% of the cases diagnosed have already spread to the lymph nodes, at which point children with this disease typically don't live past 10 years of age.[1-3]

The high mortality rate of this disease can be attributed to differences in the development of neuroblastoma from many other types of cancer.[4] Neuroblastoma arises from failure of neural crest cell precursors to differentiate, which inhibits the maturation of these cells, leaving immortal, infant malignacies, as seen in **Figure 1**.[4] During neural crest formation, the maturation process requires cascade signaling to activate transcription factors and other ligands that allow neural crest precursors to gain multipotent differentiation potential and a self-renewing phenotype.[4] This effectively drives these precursor cells into a variety of mature cells in the sympathetic nervous system, including the neurite.[4] The disruption of this maturation process transforms neural crest precursors into malignant cells.[4]

One of the challenges in treating neuroblastoma is that the tumors are inherently heterogeneous in both genotype and phenotype. Samples from different patients and even different tissues within the same patient show very different responses to their environment and to treatments.[5] The phenomenon of heterogeneity in neuroblastoma cells is supported by the so-called "multiple-hit hypothesis", which posits that cancer cells accumulate mutations as they proliferate, altering their genotype and phenotype.[6, 7] As neuroblastoma cells divide, they acquire different genetic alterations within cells of the same population. The innate heterogeneity of neuroblastoma tumors means that strict experimental parameters should be considered in order to more accurately understand the array of responses to treatment.[5] Identifying how specific molecular mechanisms relate to tumor behavior is an important step in developing an effective treatment for neuroblastoma.[5]

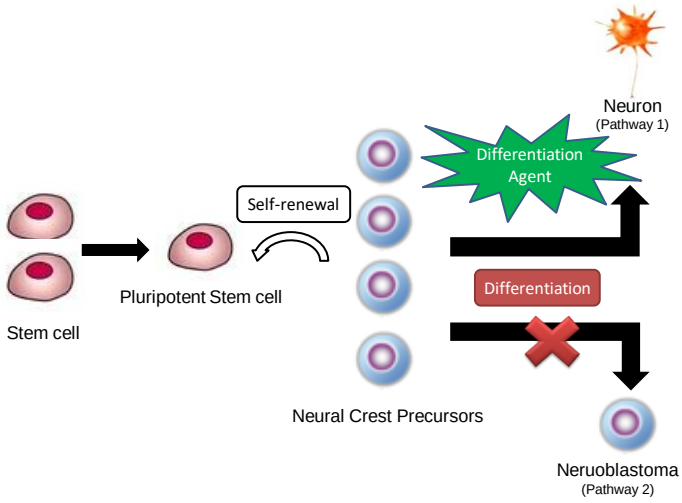

Figure 1. Neural Crest Precursor Pathway in Normal versus Neuroblastoma Cells. The lineage of the neural crest cell begins with stem cells, which can regenerate into pluripotent stem cells. These self-renewing cells can then differentiate into neural crest cell precursors. In neuroblastoma, these cells do not differentiate into neurons, and remain as infant, malignant cells (pathway 2). Differentiation agents induce neuroblastoma precursor cells to mature into neurons, and eventually undergo apoptosis (pathway 1).

1.2 Differentiation Therapy

The identification of new targets involved in differentiation provides a crucial role in the elucidation of neuroblastoma and the mechanisms of this disease.[8] The underlying development of neuroblastoma is thought to arise from disturbances in differentiation, caused by the failure of neural crest cell precursors to differentiate, which provides a foundation for differentiation therapy.[8] This therapy involves the induction of malignant cells to mature and undergo apoptosis **(Figure 1)**, and relies on the discovery of targetable biological molecules that play a role in neuroblastoma cell differentiation.[9]

Several anti-cancer drugs have been tested for efficacy of inducing differentiation in neuroblastoma, including angiogenesis inhibitors, tyrosine kinase inhibitors, demethylating agents, histone deacetylase inhibitors, heat shock protein 90 inhibitors, and retinoids.[10] For example, in 2014, Brodeur and Bagatell reported the effective use of neurotrophin inhibitors.[11, 12] The neurotrophin receptors TrkA, TrkB, and TrkC have significant roles in the development of the peripheral and central nervous systems, and in the pathogenesis of neuroblastoma, making these receptors good targets to induce differentiation in neuroblastoma cells.[11-13]

Histone deacetylase (HDAC) inhibitors have also been used to treat neuroblastoma, by deacetylating the lysine residue on the tail of histone proteins, effectively increasing the positive charge.[14-15] Modification of the histone tails affects the ability of nucleosomes to form the chromatin structure, where this influences a wide array of DNA transactions, including gene expression.[15] In 2008, Hahn *et al.* used a gene expression-based screening method involving a xenograft model to test the efficacy of HDAC inhibitors as potential enhancers of differentiation-inducing agents for neuroblastoma

treatment.[14] Retinoic acid was used alone and in combination with these HDAC inhibitors, and it was determined that the animals treated with combination therapy produced the best survival.[14] These results suggest the enhanced effect of HDAC inhibitors in combination with other agents as an effective way to treat neuroblastoma tumors, by inducing differentiation in malignant cells.[14]

It has since been determined that retinoids provide the most potent differentiation induction for neuroblastoma *in vitro.*[10] Retinoids are derived from vitamin A, and have demonstrated the ability to regulate cell proliferation, differentiation, and apoptosis in normal and in cancer cells.[16] All-*trans*-retinoic acid and 13-*cis*-retinoic acid are analogues that have been shown to produce similar activity *in vitro*.[16] Treatment with ATRA has shown a significant decrease in *MYCN* RNA expression and arrest of cell proliferation in *MYCN*-amplified and non-amplified neuroblastoma patients.[10] 13-*cis*-retinoic acid has shown clinical responses in leukemia, T-cell lymphoma, and some advanced skin carcinomas, and is effective as a single agent in preventing secondary tumors in patients with head and neck carcinoma.[10]

Neuroblastoma frequently develops chemoresistance, along with tumor recurrence arising from a resistance to ATRA that can develop after only one treatment.[17] The challenge of chemoresistance also initiates another problem, the dangerous immune suppression associated with high-dose chemotherapy.[17] This puts patients at risk for secondary infections, and ultimately makes this cancer even more difficult to treat.[17] Along with this challenge, 13-*cis*-retinoic acid treatment exhibits a 50% recurrence of the disease, providing a need for the development of new differentiation agents.[8] This is

hindered due to the poor knowledge of the mechanism of differentiation loss in neuroblastoma cells.[8]

1.3 microRNAs

MicroRNAs (miRNAs) are ~20 nucleotide long, noncoding RNAs, which have been determined to regulate transcription and the expression of many genes within the cell.[18] They bind to the 3' UTR or 5' UTR of a targeted mRNA by complementary base pairing, such that posttranscriptional gene modification may occur as translational suppression by the RNA induced silencing complex (RISC), mRNA degradation, or site-specific cleavage of an mRNA **(Figure 2).**[18, 19] Since their discovery around 1993, these naturally occurring molecules have since been connected with cancer through the modulation of gene expression of one or multiple genes.[20, 21] Over 4,000 miRNAs have been discovered so far in the human genome; many have been identified as regulators of neuroblastoma and as potential primary driving forces in controlling cell differentiation.[22] MiRNA mimics are partially double-stranded RNAs designed to augment the function of endogenous miRNAs, therefore increasing the miRNA levels in the cell.[8] These molecules have been used as tumor suppressors to inhibit tumor growth and in other cancer treatments **(Figure 3)**.[8]

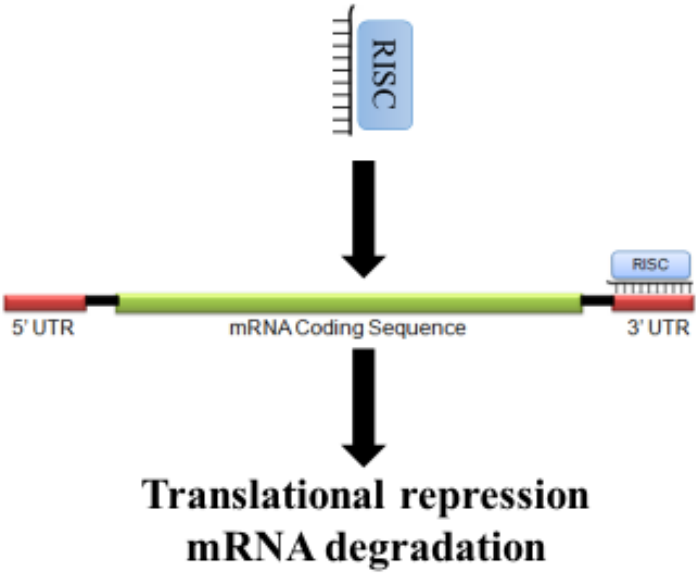

Figure 2. Effect of miRNAs in the Cell. Mature miRNAs with the RISC complex bind to the 3' UTR or 5' UTR of a targeted mRNA sequence by complementary base pairing. This leads to translational repression or mRNA degradation.

Figure 3. miRNAs as Tumor Suppressors in Cancer Therapy. Some miRNAs have been established as tumor suppressors where loss of expression in these cells leads to tumorigenicity, so miRNA mimics can be used as therapy to inhibit tumor growth by increasing the number of miRNAs in the cell.

These molecules are evolutionarily conserved and are found in loss of heterozygosity clusters throughout the entire human genome.[17] There are about 30% of human genes that are regulated by these molecules, including genes involved in

development, hematopoiesis, stress tolerance, metabolism, transcription of cellular pathways, cellular differentiation, apoptosis, stem cell maintenance, and many others.[17, 20] These molecules play critical and complex roles in controlling cellular pathways and signaling cascades, and their activity has been connected with cancer.[17]

This connection between miRNAs and cancer began with the discovery that dysregulation in these molecules leads to tumor development and metastasis, along with chemoresistance and multidrug resistance.[21-23] This recognition originated from expression profile studies, examining disruptions in signaling pathways that lead to cancer progression.[24] One of the first studies to examine this was in B cell chronic lymphocyte leukemia (B-CLL), where researchers examined the role of miRNAs and development in this cancer.[25] The study was performed by the Calin and Croce group, which used patient samples and cell lines *in vitro*, along with northern blot, western blot, and RT-PCR, to form an expression analysis of the genes contributing to B-CLL.[25] They discovered two miRNAs, *miR-15* and *miR-16*, that are down-regulated or deleted in almost 70% of CLL cases.[25] This finding led to the conclusion that miRNAs are highly regulated and involved in the genetic pathways leading to B-CLL, where they do this through tumor suppression or oncogene activation.[24, 25] The involvement of miRNAs in gene regulation contributes to the overall invasiveness and metastatic nature of this disease.[24]

1.3.1 miRNAs in Neuroblastoma Tumorigenesis and Chemoresistance

The tumorigenesis of neuroblastoma has been linked with the dysregulation of miRNAs, that have the ability to regulate expression of many genes in the genome.[20] The

dysregulation of miRNAs includes mechanisms such as translocation, mutation, deletion, and rearrangements, causing a wide array of the expression levels of miRNA in normal cells versus cancer cells.[19] In neuroblastoma, there are a variety of clinical displays, including localized and metastatic tissues.[19] Tumors arising from this disease are often metastasized to the liver, bone, brain, and skin, indicating a deeply heterogeneous nature of the disease.[19] For neuroblastoma cells to metastasize, migration and invasion are key requirements that can have a major clinical outcome on patients.[23] This disease has a correlation to specific genomic conditions, including hypodiploidy, chromosome structural abnormalities, chromosomal imbalances, *MYCN*-amplification, and others.[16] *MYCN* expression has been established as a very influential part of neuroblastomal tumor metastasis.[23] This oncogene is seen hugely over-expressed in high-risk neuroblastoma patients, and is indicative of poor patient outcome.[23] Despite these correlations, there is not much known about the specific targets of this oncogene in neuroblastoma.[23]

Neuroblastoma has commonly been shown to produce chemoresistance and relapse after even one treatment, which makes effective treatment of neuroblastoma difficult.[24] It is estimated that there is about 90% of chemotherapy failure due to resistance from metastatic cancers, which is correlated with either intrinsic or extrinsic resistance.[19] Intrinsic resistance refers to cancer cells that are innately resistant to chemotherapy, while extrinsic resistance refers to cancer cells that acquire a resistance to chemotherapy through genetic or epigenetic mutations with multiple chemotherapy treatments.[19] In both cases, chemoresistnace is directly related to a poor prognosis.[19] The problem of chemoresistance can be attributed to miRNAs that regulate genes involved in initiating this resistance mechanism.[25] One hypothesis for the high resistance to chemotherapy

drugs seen in neuroblastoma cells has been attributed to the fact that miRNAs may be able to affect processes like drug metabolism pathways or efflux pumps.[25] This allows neuroblastoma cells to acquire a resistant phenotype, and includes change in expression of tyrosine kinases, glycoproteins, growth factor receptors, and others that contribute to this.[25]

1.3.2 miRNAs in Neuroblastoma Differentiation and Therapy

MicroRNAs have been suggested as therapeutic targets for neuroblastoma.[23-28] This is because miRNA expression plays a role in tumorigenesis, metastasis, chemoresistance, proliferation, invasion, migration, and other key processes involved in the overall aggressiveness of this disease.[23-28] These are indicative of the overall patient background and outcome of the disease.[26] MiRNA mimics have been well studied in neuroblastoma cell differentiation, and may be used to modulate the level of these molecules in the cell.[28] This addition of miRNA mimic changes the expression profile and provides possible uses in diagnostics, prognostics, and overall therapy for neuroblastoma patients.[24] The effects of these molecules on neuroblastoma cells (i.e. tumorigenicity, pathogenesis, differentiation, etc.) have been well documented.[27, 30-45]

For example, a study in 2007 by Chen and Stallings used high-throughput screening techniques to perform miRNA profiling studies in neuroblastoma.[27] They analyed miRNA expression *in vitro* in 157 primary neuroblastoma tumors, and found that 32 miRNAs presented differential expression (i.e., up- and down-regulation).[27] Their data suggests roles for miRNAs in the pathogenesis and apoptosis of this disease, along with the potential therapeutic roles of miRNAs.[27]

Some other miRNAs have been sequenced to determine differential expression in neuroblastoma cells.[29] A study performed by Einvik *et al.,* examined the expression of 43 miRNAs at diagnosis and at relapse of several neuroblastoma patients.[29] It was observed that 8 miRNAs were upregulated, while 34 were downregulated.[29] 22 of the downregulated miRNAs were consistently associated with poor patient prognosis and observed as consistent in over 220 neuroblastoma tumors.[29] A pathway analysis program, Ingenuity Pathway Analysis (IPA), was then used to predict the possible target genes associated with this miRNA expression profile.[29] Among the wide array of results, many of the target genes from this miRNA expression profile were seen to be correlated with cancer cell progression and/or drug resistance.[29] These results suggest that the downregulation of many miRNAs in neuroblastoma cells may contribute to the overall cancer progression, and that miRNAs may be used as possible neuroblastoma therapy.[29]

In 2015, Du *et al.* showed that a novel miRNA, miR-449a, functions as a tumor suppressor and potent inducer of differentiation in neuroblastoma and other cancers.[40] Two mechanisms were discovered that produced the inhibition of neuroblastoma cell growth, including the induction of differentiation and cell cycle arrest.[40] This study examined five target genes, *MFAP4*, *PKP4*, *TSEN15*, *CDK4*, and *LEF1*. The first three of these genes are important for the differentiation of neuroblastoma cells, while the last two genes are important for inducing cell cycle arrest.[40] The tumor expression levels showed high gene expression for the three miR-449a target genes, but no significant change was observed in the two target genes for cell cycle arrest. Furthermore, miR-449a was shown to possess tumor suppressor abilities, such that the induction of differentiation may improve the prognosis of neuroblastoma patients.[40]

Several proteins involved in alternative splicing have been found to play a key role in neuroblastoma cell differentiation through nervous system development.[36] This was observed in a study done by Maniatis *et al.*, where miR-124 was transfected into neuroblastoma cells *in vitro*.[36] Following this treatment, a gene expression microarray was performed.[36] It was determined that PTBP1, a splicing repressor, and PTBP2 were seen highly downregulated in these cells, and were determined to be direct targets of miR-124.[36] The results of this study expose the crucial role of miR-124 in the differentiation and maturation of neuroblastoma cells.[36] They also suggest this miRNA as a possible therapeutic agent to treat this cancer.[36]

A study performed by Caffarelli *et al.*, investigated an isoform of neurotrophin receptor tropomyosin-related kinase C (*TRKc*) that was seen highly repressed in neuroblastoma cells *in vitro* after the ectopic expression of miR125a/b and miR-9.[48] The study examined the expression of these miRNAs in neuroblastoma cells, and observed a highly downregulated expression of *TRKc* in all three miRNAs.[48] The downregulation of *TRKc* was determined to play a critical role in neuronal differentiation and growth of these cells.[48] These observations together indicate an important role of these miRNAs in neuroblastoma cell growth, and in overall neuroblastoma cell differentiation.[48]

MiRNA-184, a pro-apoptotic miRNA and direct downstream target of *MYCN*, was observed to directly target AKT2, and therefore the phosphatidylinositol 3-kinase (PI3K) pathway, in a study performed by Stallings *et al.*[49] Following siRNA knockdown of this miRNA, the number of neuroblastoma cell lines was increased *in vitro*.[49] The same effect on neuroblastoma cell number was observed when ectopically upregulating AKT2, a direct target of this miRNA.[49] As further confirmation, the co-transcription of miR-184

from an AKT2 vector lacking the 3' UTR for miR-184 produced an inhibition in the pro-apoptotic effect of this miRNA.[49] These observations suggest that miR-184 may be used as a possible therapeutic agent in high-risk neuroblastoma patients with *MYCN* amplification, through targeting AKT2 and effectively reducing cancer cell survival.[49]

Another study examined the expression profile of a specific miRNA, miR-338-3p, and its target gene, apoptosis-associated tyrosine kinase (AATK), upon transfection of this miRNA into neuroblastoma cells.[50] The expression of miR-338-3p *in vitro* significantly decreased AATK, revealing a key role for this miRNA and its target gene in neuroblastoma cell differentiation.[50] This suggests a possible therapeutic mechanism that this miRNA could have on neuroblastoma cell differentiation.[50]

Other miRNAs have been discovered to induce malignant cells to mature and undergo apoptosis.[18] In 2012, Stallings *et al.* performed the first *in vivo* study in a murine orthotopic xenograft model, to determine if miRNAs are involved in the suppression of tumor growth in neuroblastoma.[33] They used miR-34a, a potent miRNA mimic for apoptosis, and silica nanoparticles, to test levels of GD2, a cell surface antigen, in primary neuroblastoma tumors.[33] After conjugating the GD2-antibodies to the nanoparticles, and performing western blots, RT-PCR, and several other methods, they injected these nanoparticles into the animal models.[33] The results of this study provided evidence for a reduction of angiogenesis, an increase in apoptosis, and an overall significant decrease in tumor growth, therefore demonstrating the physiological and biological effects of miRNA mimics on neuroblastoma tumorigenesis.[33]

There is also some evidence of conflicting results with regards to the function of specific miRNAs involved in the differentiation of neuroblastoma.[28, 44] For example,

miR-10a and miR-10b have been reported as both inducers and inhibitors of differentiation.[28, 44] A 2011 study performed by Stallings *et al*. concluded that these miRNAs are involved in the induction of differentiation, while a 2014 study by Du *et al*. revealed a conflicting result, that *miR-10a* and *miR-10b* inhibit differentiation in neuroblastoma.[28, 44] This indicates a need for further research and standard techniques to be used in the elucidation of miRNAs' involvement in the expression of gene regulation in neuroblastoma.

Despite some conflicting results, there is overwhelming evidence that miRNAs are outstanding mechanisms for differentiation therapy in neuroblastoma, by inducing malignant cells to mature and undergo apoptosis.[20, 21, 27, 32, 46]

1.3.3 miRNA-506-3p Induces Cell Differentiation in Neuroblastoma

Du *et al.* used a high-content screening technique that allows for the visualization of cells by using either genetically engineered cell lines expressing fluorescent signals or the staining of fixed cells.[8] It examines neurite outgrowth, an easily detectable morphological feature of neuroblastoma cells, to directly identify miRNAs that induce neuroblastoma cell differentiation.[8] Using this improved technique, a group of 14 novel miRNAs that induce neuroblastoma cell differentiation were identified by Du *et al*.[8] This group identified novel miRNAs that induce differentiation and may be possible anti-cancer drug targets.[8] One specific miRNA, miR-506-3p, was identified as the most potent miRNA and was found to be highly regulated in neuroblastoma cells, suggesting that this miRNA may be a major contributor in controlling cell differentiation and the reduction of cell growth and survival.[8] MiR-506-3p was shown to down-regulate two main predicted

targets, CDK4 and STAT3, at the target sites in the 3' UTR regions of these genes, as shown by a luciferase reporter assay.[8] The down-regulation of these proteins' levels effectively reduced neurite outgrowth, whereas the combined repression enhanced neurite outgrowth relative to individual repression.[8] MiR-506-3p also showed a more potent effect than 13-*cis*-retinoic acid, which suggests this miRNA as an effective differentiation agent for neuroblastomal remission therapy.[8]

1.4 Project Aims

This study aimed to experimentally determine the effects of miR-506-3p mimic on undifferentiated neuroblastoma cells, in anticipation of providing preliminary evidence for the use of this miRNA mimic as possible differentiation therapy in neuroblastoma patients. The first aim of this study was to determine whether miR-506-3p mimic has a more general differentiation-inducing effect on neuroblastoma cells than retinoic acid. This was done by examining the correlation of cell sensitivity to retinoic acid and the miR-506-3p mimic in a panel of neuroblastoma cell lines with distinct genetic backgrounds. This required several steps, including (1) determining the response to ATRA in neuroblastoma cell lines with different genetic alterations, (2) determining the response to the miR-506-3p mimic in the same neuroblastoma cell lines, and (3) determining the correlation between ATRA and the miR-506-3p mimic sensitivity. The second aim was to determine if the combined treatment of ATRA and the miR-506-3p mimic synergistically promoted neuroblastoma cell differentiation.

To do this, several techniques were used to analyze the overall effects on neuroblastoma cell differentiation. These techniques included cell culture, direct and reverse transfections, neurite outgrowth assays, MTT assays, cell proliferation assays, and Western Blots. Together these techniques allowed for a quantitative evaluation of the responses to all the treatments, alone and in combination, on a panel of diverse neuroblastoma cell lines.

The hypotheses of this study were (1) the miR-506-3p mimic will have a broader differentiation-inducing effect on neuroblastoma cell lines than retinoic acid, and (2) the combined treatment with retinoic acid and the miR-506-3p mimic will produce an enhanced effect on neuroblastoma cell viability.

II. MATERIALS AND METHODS

2.1 Materials and Reagents

The materials and reagents used in this project are listed below:

Materials (Catalogue NO.)	**Company**
Acrylamide/Bis-Acrylamide 29:1 40% solution	Fisher
Albumin Standard	Pierce BCA Assay
Ammonium peroxidase	Fisher
ATRA	Sigma
Bromophenol Blue	Fisher
Crystal Violet Stain (AC405831000)	Fisher
Dharmacon microRNA mimics & control oligos	Fisher
DMEM	Fisher (MT-10092CM)
DMSO	Fisher (BP2311-CS)
DPBS	Fisher (21-031-CV)
FBS	Atlas Biologicals (EF-0500-A)
Glycerol	Fisher
HCl	Fisher
KCl	Fisher
LipofectamineRNAiMax	Fisher (13778150)
Methanol	Fisher (A947-4)
MTT Reagent	Fisher (074E306168)
NaOH 1%	Corning (10-090-CV)
NaCl	Fisher
Non-Fat Powdered Milk (P-1400)	Boston BioProducts
Penicillin-Streptomycin	Fisher (15-140-122)
Pierce BCA Assay Reagent A	Fisher (23228)
Pierce BCA Assay Reagent B	Fisher (1859078)
PVDF membranes	Fisher (88518)
Rabbit anti-GAP43, anti-NSE, and anti-Beta Tubulin III	Abcam
Rabbit anti-Calnexin and goat anti-rabbit secondary antibody conjugated with horseradish peroxidase (HRP)	Sigma (P8250-5KU)

Running Buffer 1X	National Diagnostics (EC-870)
Spectra multicolor broad range protein ladder	Fisher (26634)
SuperSignal West Dura	Fisher (PIA34075)
SuperSignal West Pico	Fisher (34080)
TEMED	Fisher
Transfer Buffer 1X	National Diagnostics (EC-880)
Tris	Fisher
Trypsin	Fisher (25-052-Cl)
Tween 20	Fisher
2-mercaptoethanol	Fisher

All other items were obtained from Fisher.

The miRNA mimic sequence synthesized by Dharmacon is listed below:

miRNA mimic	**Sequence with target site**
miR-506-3p	UAAGGCACCCUUCUGAGUAGA

The control oligomer used in this project were provided by Dharmacon, and contain a random sequence that does not bind to the mRNA transcript.

2.2 Software and Equipment

The software and equipment used in this project are listed below:

Software	**Company/Location**
Canon CanoScan 9000F MarkII	Aurora, IL, USA
Canon ScanGear Tool Software 64bit Windows 7	Bangrak, Bandkok, Thailand
ChemiDocXRS+ System	BioRad, Hercules, CS, USA
GraphPad Prism 7.01	GraphPad Software, La Jolla, CA, USA
ImageJ	NIH, Bethesda, MD
ImageLab Software model ChemiDoc XRS+	BioRad, Hercules, CA, USA
Mini-PROTEAN Tetra 10025025 - RevA 12-0625 0312	BioRad, Hercules, CA, USA
NeuroTrack System	Essen Bioscience, Ann Arbor, MI, USA
Synergy H4 Hybrid Microplate Reader	BioTek, Winooski, VT, USA

ZOOM IncuCyte Imaging System Essen Bioscience, Ann Arbor, MI, USA

2.3 Cell Lines

BE(2)-C, SK-N-SH, SK-N, BE(2), SK-N-AS, SK-N-F1, BE(2)-M17, CHP-212, SK-N-DZ, SK-N-MC, SH-SY5Y, NGP, IMR-32, and MC-IXC cells were obtained from the American Type Culture Collection (ATCC). CHLA-90 and SK-N-BE cells were obtained from Children's Oncology Group (COG). Kelly cells were purchased from the cell line repository at the Greehey Children's Cancer Research Institute, University of Texas Health Science Center (San Antonio, TX, USA). The genetic backgrounds of the neuroblastoma cell lines used here are listed in **Table 1**.

Table 1. The Diverse Genetic Alterations of Neuroblastoma Cell Lines used in this Project. The neuroblastoma cell lines used in this study are diverse, and show a wide array of different genetic alterations, such as MYCN amplification, p53 status, TH expression, and chromosome alterations. Some of the information is not available (NA).

NB Cell Lines	MYCN expression	p53 Status	TH Expression	Chromosome Alterations	1p alteration
BE(2)-C	amplified	non-functional	expressed	NA	NA
Kelly	amplified	normal	NA	yes	NA
CHLA-90	non-amplified	non-functional	expressed	NA	NA
SK-N-DZ	amplified	normal	NA	yes	NA
SK-N-F1	amplified	NA	expressed	NA	NA
SK-N-BE(2)	amplified	non-functional	expressed	yes	yes
SK-N-AS	non-amplified	NA	NA	yes	yes
BE(2)-M17	amplified	NA	NA	NA	NA
CHP-212	amplified	NA	NA	NA	NA
SH-SY5Y	amplified	NA	NA	NA	NA
MC-IXC	non-amplified	NA	NA	yes	NA
IMR-32	amplified	NA	NA	yes	yes
SK-N-MC	amplified	NA	NA	yes	NA
SK-N-SH	non-amplified	NA	NA	yes	no
NGP	amplified	NA	NA	yes	yes

2.4 Cell Culture

Cell lines were grown in DMEM supplemented with 10% fetal bovine serum and 5% penicillin streptomycin antibiotic. Cells were passaged every 3-4 days, with a limit of 20 passages for experimental use (to control for the innate heterogeneity of neuroblastoma cells mentioned in Chapter I). To passage the cells, the media was discarded and 2 mL of warmed (37°C) DPBS was added to wash the cells. The DPBS was then discarded and 2 mL of warmed (37°C) trypsin was added to detach the cells from the dish, which was then placed in the CO_2 incubator at 37°C for 3-5 minutes. Then, 2 mL of warmed, full media was added to the dish to neutralize the trypsin, and gently pipetted to break the cell clumps. The cells were then transferred into a 15 mL tube and spun down for 3 minutes. Next, the supernatant was discarded and 5 mL of fresh, warm, full media was added to resuspend the cells. Finally, the cells are transferred to 100 mm dishes with a new passage number.

Cell counting was performed with a hemocytometer, where the cells were observed and counted in the five sets of 16 squares on the corners of the grid. Calculating the number of viable cells per milliliter involves taking the average number of cells and multiplying by 10,000 (10^4) and then by five to account for the 1:5 dilution from the Trypan Blue to give the total number of viable cells in the original suspension.

2.5 Transfections

2.5.1 Reverse Transfection for Neurite Outgrowth Assay

Following cell splitting, the cells were counted with a hemocytometer and calculations performed such that approximately 2,500 cells per well were plated in 96-

well plates. After cell counting, the working cell mixture was prepared in incomplete media (DMEM with 15% FBS) in Eppendorf tubes. Then 1 μL of miRNA mimics and/or control oligos were placed in each well at 2.5 nM concentration. Next, the Lipofectamine RNAimax liposome was prepared in plain media in new Eppendorf tubes, and after incubation for 5 minutes at room temperature, approximately 30 μL per well were added to the plate. The plate was then mixed well with the vortex, and incubated for approximately 20 minutes at room temperature, during which the plate was vortexed again and spun down for 5 minutes. To aid the liposome-miRNA mimic fusion, the plates were vortexed and spun down again, and then 100 μL of cells from the working cell mixture was carefully added to each well. The plate was then placed in the ZOOM IncuCyte NeuroTrack Imaging System. After 24 hours, 70 μL of full media was added to each well and considered as "day 1". If combined treatment with ATRA was required, this was added with the 70 μL of full media, and the plate was placed back into the imaging system for approximately 120 hours.

2.5.2 Reverse Transfection for Colony Formation Assay

Following cell splitting, the cells were counted with the hemocytometer and calculations performed such that approximately 2,000 (for BE(2)-C cells) or 4,000 (for Kelly and CHLA-90) cells per dish were plated on 100 mm dishes. After cell counting, the working cell mixture was prepared in plain media in Eppendorf tubes. Then, 18 μL (per plate) of the miRNA mimics and/or control oligos were added to a separate set of Eppendorf tubes with 180 μL (per plate) of plain media. These tubes were mixed well with the vortex, and incubated for 5 minutes at room temperature. Next, 1.8 μL of the Lipofectamine RNAimax liposome stock was added to the tubes. The tubes were mixed

well with the vortex, and incubated for 20 minutes at room temperature to allow for the uptake of the miRNA mimics and/or control oligos to be taken-up into the liposomes. After this incubation period, these tubes are added to the corresponding working cell tubes, and placed on a rocker for approximately 2 hours at room temperature. In new 50 mL tubes, 31 mL of full media was combined with the corresponding tubes after the incubation period. The tubes were inverted several times to mix, and 10 mL aliquots plated on 100 mm dishes and placed in the CO_2 incubator at 37°C for approximately 2 weeks. The colonies were observed from the bottom of the dishes as white dots throughout this incubation period, and once the colonies are determined as big enough, they were stained. To do this, the cell media was discarded and the plates were washed with DPBS several times to remove the culture media. After discarding the DPBS, approximately 5 mL per dish of crystal violet stain was added to the dishes and incubated for 20 minutes at room temperature. Following incubation, the crystal violet stain was discarded, and the plates were soaked in tap water for approximately one minute to remove any remaining stain. The plates were prepared for imaging by drying upside down and without lids overnight. Imaging was performed by placing the plates face-down and without lids on the Canon CanoScan 9000F MarkII scanner for colony counting. Statistical analysis was performed as seen below.

2.5.3 Forward Transfection for Western Blot

Following cell splitting, the cells were counted with the hemocytometer and calculations performed such that approximately 60,000 cells per dish were plated on 60 mm dishes. After 24 hours, Eppendorf tubes are prepared with 650 µL of plain media and 18 µL of the miRNA mimics or control oligos. The tubes are mixed well with the vortex,

and incubated for 5 minutes at room temperature. Then, 2.5 μL of the Lipofectamine RNAimax liposome were added to each tube, mixed well with the vortex, and incubated for approximately 20 minutes at room temperature. During the incubation period, the culture media was discarded from the dishes, 2 mL of plain media was added to wash the cells and discarded again. Then, 500 μL of plain media was added to each dish, and after the incubation period was complete, the liposomes were added dropwise to the dishes. The dishes were swirled well to mix and placed in the CO_2 incubator at 37°C for approximately 2 hours. After this incubation period, 2 mL of full culture media was added to the dishes. If combined treatment with ATRA was required, this was added with the 2 mL of full media, and the dishes were placed back into the incubator for approximately 120 hours until sufficient cell growth for cell lysate collection. The Western Blot technique was performed as described below.

2.6 Detection and Quantification of Neurite Outgrowth

Cells were plated and treated with ATRA or transfected with miRNA mimics in 96-well plates before being placed in the ZOOM IncuCyte Imaging System (as described above), where the cell images were taken under 20X microscopic magnification. To detect neurite outgrowth, images were taken every 6 hours for 120 hours. The neurite outgrowth lengths for each treatment were calculated using a neurite definition defined for each specific cell line with the NeuroTrack system, and statistical analysis was performed as described below.

2.7 MTT Assay (Cell Viability Assay)

After treatment from the neurite outgrowth assay in a 96-well plate (as described above), the cells were cultured for approximately 5 days and the cell viability was determined using an MTT Assay. After sufficient cell growth (120 hours), 15 μL of MTT Reagent was added to each well, and plates were placed in the CO_2 incubator at 37°C for 1-5 hours (until crystal formation has occurred). The plate was then spun down for 5 minutes, and the media was dumped in the sink. To dissolve the crystals, 50 μL of DMSO was added per well, and incubated for approximately 15 minutes at 37°C. The plate was then imaged with the Synergy H4 Hybrid Microplate Reader according to the manual, at both 630 nm and 570 nm. The values associated with the 570 nm range were first subtracted from the values associated with the 630 nm range, and the statistical analysis was performed as described below.

2.8 Colony Formation Assay (Cell Proliferation Assay)

Cells were plated and treated with ATRA or transfected with miRNA mimics in 100 mm dishes (as described above), and after 2 weeks the cells were visualized using 1% crystal violet staining. The number of colonies and average size of the colonies were analyzed using the automated colony counter and ImageJ software, with the statistical analysis described below.

2.9 Western Blot

The general procedure performed included cell treatment, preparation of the cell lysate, BCA assay to determine protein concentration, preparation of samples and mini-gels for SDS-PAGE, running of the SDS-PAGE, transferring the protein to a PVDF membrane, blotting the membranes, and re-blotting the membranes (if required for confirmation of loading control).

2.9.1 Cell Lysate Preparation and BCA Assay

Preparation of the cell lysate began with plating the cells and treating with ATRA or transfecting with miRNA mimics in 100 mm dishes (as described above), and growing the cells for 120 hours. The cell lysates were collected beginning with discarding the media from the dishes and washing with 1X DPBS four times to remove any remaining media. The dishes were then dried for approximately 3 minutes at -20°C, and 50 µL of lysis buffer was added to each dish. Next, the dishes were scraped and the cell lysate collected in Eppendorf tubes. The tubes were placed on ice at 4°C for 10 minutes, and spun down (at max speed) with the microcentrifuge for 5 minutes to spin down the cell debris. Next, the supernatant was transferred to new Eppendorf tubes for BCA assay. The BCA assay was set up in 96-well plates, where reagent A and B were prepared in a 50:1 ratio. Sample wells contained 200 µL of BCA mixture and 2 µL of sample supernatant; the standard well contained 200 µL of BCA mixture and 5 µL of Albumin Standard (1 mg/mL BSA), and the blank well contained just 200 µL of the BCA mixture. The plate was then incubated for approximately 15-30 minutes at 37°C (until the green color changed to purple). Plates were then imaged at 562 nm with the Synergy H4 Hybrid

Microplate Reader. The protein concentrations were determined using Excel, where the absorbance value at 562 nm was subtracted from the absorbance value of the blank standard from all the other 562 nm measurements of the individual standard or unknown sample replicates. The protein concentration of each sample was determined using the average blank-corrected 562 nm measurement for the standard and unknown samples. The volume for 10-20 μg of protein was calculated for sample loading to the SDS-PAGE mini-gels. Then, 5X protein loading buffer was added to the supernatant tubes at ¼ of the supernatant volume. The tubes were placed on the heat block for 5 minutes at 90°C, and then stored at room temperature for immediate use (i.e., same day), -4°C for short-term storage (i.e., up to several months), or -20°C for long-term storage (i.e., for years). A final set of Eppendorf tubes were prepared to load the mini-gels by mixing the calculated volume of cell lysate with 1X protein loading buffer, and also a tube prepared with 5 μL (per gel) of multicolored protein ladder mixed with the matched volume of 1X protein loading buffer.

2.9.2 SDS-PAGE

After preparation of the (lower) 10% acrylamide resolving gel in 50 mL tubes, approximately 4.6 mL was added/poured to the plates, sprayed with 70% ethanol to remove any air bubbles, and allowed to polymerize for up to 30 minutes. After pouring off the ethanol, the (upper) 4% acrylamide stacking gel was prepared and added/poured onto the top of the lower gels. Then, a 10 or 15-well comb was placed on top of the upper gels and allowed to polymerize for up to 45 minutes. Once polymerization of the gels was complete, the plates were placed into the cassettes with the short-plates on the inside. 1X

running buffer (0.25 M Tris, 1.92 M glycine, 1% SDS) was poured inside the cassettes, and the combs were removed for loading. Equal amounts of the cell lysate protein and the protein ladder were loaded into the mini-gels (1.0 mm), and resolved by the SDS-PAGE for electrophoresis. The SDS-PAGE was run at 120 volts for 40 minutes with the Mini-PROTEAN Tetra System until the blue dye reached the bottom of the mini-gels.

2.9.3 Transfer

After completion of the SDS-PAGE, the apparatus was taken apart, and gel-sized (3.0 X 3.8 in) Immun-Blot PVDF membranes were rocked first in methanol for 5 minutes and then in cold 1X transfer buffer for 5 minutes. The gels were then cut and washed up to 5 times with tap water to remove the SDS-PAGE, placed in 1X transfer buffer (0.25 M Tris, 1.92 M glycine), and aligned on the membranes to make the sandwich. The sandwich was placed into the transfer container with an ice pack, and filled with 1X transfer buffer. This container was placed on ice and run with transfer conditions set to 200 mA for 2 hours (for 2 membranes) with the Mini-PROTEAN Tetra. Upon completion of the transfer, the apparatus was taken apart and the membranes placed on a wet paper towel with dH_2O for trimming. The membranes were then trimmed and rocked in cold blocking buffer for 30 minutes to 1 hour. (Note: the membranes were handled with clean gloves and tweezers as to prevent contamination.)

2.9.4 Blotting

After blocking, the membranes were washed up to four times with TBST wash buffer and incubated with 1 mL of primary antibodies on a parafilm-covered plate for either one hour at room temperature or overnight at 4°C for specific differentiation

markers (i.e. rabbit anti-Calnexin, rabbit anti-Beta Tubulin III, rabbit anti-GAP43, and rabbit anti-NSE). The membranes were again washed up to four times with TBST wash buffer, and placed into a blotting box with approximately 5 mL of the secondary antibody solution. The bound primary antibodies were detected using secondary antibodies goat anti-rabbit conjugated with horseradish peroxidase (HRP) for 1 hour at room temperature. The membranes were again washed up to four times with TBST wash buffer and rocked with SuperSignal West Pico/Dura Chemiluminescent Substrate for 5 minutes at room temperature. The membranes were individually visualized with ImageLab software connected to the ChemiDocXRS+ System, and used according to the manual.

2.9.5 Re-blotting

Re-blotting began with washing the membranes up to four times with TBST wash buffer and then rocked in stripping buffer (1% NaOH) for approximately 30-45 minutes at room temperature. The membranes were then rocked in blocking buffer for 30 minutes to 1 hour, and re-blotted with primary and secondary antibodies as described above. The PVDF membranes were re-blotted up to three times, and stored dry at room temperature for up to several years.

2.9.6 Recipes

The recipes for each of the specific solutions used in the Western Blot are listed below:

Acrylamide mini-gels (1.0 mm; 2 gels):

	Resolving Gel				Stacking Gel
	8%	10%	12%		4%
dH20	5.45 mL	4.95 mL	4.45 mL		3.25 mL
lower Tris, pH 8.8 (1.5M Tris, 0.4% SDS)	2.5 mL	2.5 mL	2.5 mL		1.25mL
40% acrylamide/bis	2.0 mL	2.5 mL	3 mL		0.5 mL
10% ammonium persulfate	100 µL	100 µL	100 µL		50 µL
TEMED	10 µL	10 µL	10 µL		5 µL

Antibody Buffer (5-10 mL): 1X TBS, 0.5% dry milk, 0.05% Tween 20
Blocking Buffer (45 mL): 1X TBS, 5% dry milk, 0.05% Tween 20
Cell Lysis Buffer (15 mL): 25 mM Tris, 2.7 mM KCl, 137 mM NaCl, pH adjustment to 7.4, 1% Triton X-100 (protease inhibitor was added before use, and stored at -20°C after use)
Primary Antibodies (1 mL at 1:1000 dilution): 1 µL primary antibody, 1 mL antibody buffer
Protein Loading Buffer 5X (20 mL): 3.2 mL of 2M Tris-HCl at pH 6.8, 4.3 mL of dH_2O, 10 mL glycerol, 1.0 mg bromophenol blue, 2.0 g SDS, 2.5 mL 2-mercaptoethanol
Running Buffer 1X (1 L): 3 g Tris, 14.4 g glycine, 1 g SDS
Secondary Antibodies (45 mL at 1:10,000 dilution): 4.5 µL secondary antibody solution, 5 mL blocking buffer, 40 mL TBST wash buffer
TBS Buffer 10X (2 L): 48.46 g of 200 mM Tris ad adjust to pH 7.6, 175.32 g of 150 mM NaCl, 30 mL HCl and adjust to pH 7.4
TBST Wash Buffer (1 L): 1X TBS, 0.05% Tween 20, dH_2O
Transfer Buffer 1X (1 L): 3.03 g of 25 mM Tris, 14.41 g of 192 mM glycine (do not adjust pH)
West Pico Chemiluminescent Substrate (10 mL): 5 mL of reagent A, 5 mL of reagent B

2.9.7 Quantification

To determine the protein expression from the effect of ATRA and/or miRNAs on neuroblastoma cell differentiation, ImageJ software was used. This software assigned values based on lane intensity, which were then normalized to the control and to the loading control.

2.10 Statistical Analyses

2.10.1 Neurite Outgrowth Assay

To determine the effect of the ATRA, miRNAs, or combined treatment on neurite outgrowth, the *p*-values of the neurite lengths associated with the miRNAs was compared with the neurite lengths of the negative control oligos with a two-sample t-test. The statistical significance was determined by comparing the treatment group with the control using GraphPad Prism 7, with $P < 0.05$ considered statistically significant. GraphPad Prism 7 defines the p-values as follows:

Symbol	**P-value**
*	$P \leq 0.05$
**	$P \leq 0.01$
***	$P \leq 0.001$
****	$P \leq 0.0001$

2.10.2 MTT Assay

To determine the effect of the combined treatment of ATRA and the miRNAs on cell viability, the Bliss Independence Model was performed after the above mentioned two-sample t-test using GraphPad Prism 7 with $P < 0.05$ as considered statistically significant. The Bliss Independence Model was used to calculate the predicted additivity with the formula, $E_{xy} = E_x + E_y – E_xE_y$, where E_x was the individual effect of the ATRA on neuroblastoma cell viability, E_y was the individual effect of the miRNAs on neuroblastoma cell viability, E_xE_y was the additive effect on neuroblastoma cell viability, and E_{xy} was the calculated predicted additivity .[50, 51]

2.10.3 Colony Formation Assay

To determine the effect of the ATRA and/or miRNAs on cell proliferation, ImageJ software was used, which assigned values based on an automated colony counter that estimates the average number of colonies and the average colony size. These values are then used to perform a two-sample t-test as mentioned above. The statistical significance was determined by comparing the treatment group with the control group using GraphPad Prism 7, with $P < 0.05$ considered statistically significant.

III. RESULTS AND DISCUSSION

3.1 Introduction to Results

Although the discovery of miRNAs is recent, they play a crucial role in regulating essential physiological processes including development, proliferation, migration, apoptosis, invasion, angiogenesis, differentiation, tumorigenesis, metastasis, and chemoresistance.[16, 17, 46] Despite their prevalence, there still remains a gap in knowledge needed to use miRNAs as therapy for the treatment of neuroblastoma and other cancers.[8] Recant current insights into the functions of miRNAs have provided awareness into some of the knowledge needed to fill this gap, but has still left challenges that must be overcome for the use of predicted therapeutics.[8] These challenges include understanding the specific mechanisms of miRNAs, the connections between these molecules and gene expression, and their contribution to tumorigenesis, metastasis, and chemoresistance.[8] To address these challenges, further research into miRNAs and their involvement in these processes is needed, since there have been no reports comprehensively investigating the functions of miRNA species in neuroblastoma differentiation.[8]

As stated in Chapter I, the first major goal of this project was to determine the correlation of neuroblastoma cell sensitivity to retinoic acid and the miR-506-3p mimic, which involved three steps, including determining the response to ATRA in neuroblastoma cell lines with different genetic alterations; determining the response to the miR-506-3p mimic in the same neuroblastoma cell lines; and determining the correlation between ATRA and the miR-506-3p mimic sensitivity. The second goal was

to determine whether combined treatment of ATRA and the miR-506-3p mimic have a synergistic effect on neuroblastoma cell viability.

Completing this project required the detection of neurite outgrowth as a morphological detection method for neuroblastoma cell differentiation, developed by Du *et al*.[8] In addition to this, other approaches were used to confirm neuroblastoma cell differentiation, such as cell viability and cell proliferation assays, along with the detection of molecular differentiation markers (GAP43, β (III) Tubulin, and NSE) by Western Blot, with calnexin as a loading control.

Figure 4 shows the confirmation of the IC_{50} of ATRA treatment (at 5 μM) in BE(2)-C cells, indicating the amount of ATRA needed for 50% cell death following treatment, as reported by Du *et al*.[8] **Figure 4A** shows neurite outgrowth images following the treatment of BE(2)-C cells with two concentrations of ATRA as performed in a neurite outgrowth assay. The left image shows control cells with no ATRA treatment, the middle image shows 2.5 μM of ATRA treatment, and the right image shows 5 μM ATRA treatment. Observing the images from left to right, it is evident that there is a reduction in cell body area (yellow) and an increase in neurite outgrowth (purple). **Figure 4B** shows the analysis following an MTT assay performed to determine the cell viability of BE(2)-C cells after these treatments. The data shows a statistically significant reduction in both the 2.5 μM and 5 μM ATRA treatments as compared to the control group, but only a 50% reduction in viability after the 5 μM treatment. These results confirm the previously reported IC_{50} of 5 μM ATRA treatment in BE(2)-C cells resulting in 50% cell death.[8]

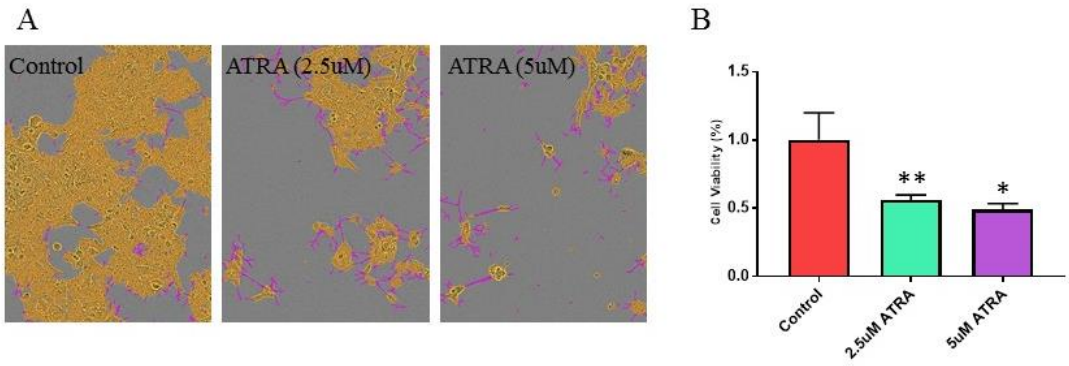

Figure 4. The Confirmation of the IC_{50} of ATRA in BE(2)-C Cells. The confirmation of the IC_{50} of ATRA in BE(2)-C cells as seen in (A) the neurite outgrowth images and analyzed by (B) the cell viability. Neurite outgrowth images are representative of nine non-overlapping individual images from a single sample. Error bars reflect SEM of n = 3 technical replicates; * $P \leq 0.05$, ** $P \leq 0.01$.

3.2 Neuroblastoma Cell Lines with Different Genetic Background Show Varied Responses to Treatment with ATRA

3.2.1 BE(2)-C Cells

Due to limited time and resources, a single concentration of ATRA at 5 μM (from the IC_{50} previously reported in BE(2)-C cells) was chosen **(Figure 4)**.[5] From here, the first step in this project was to determine the response of neuroblastoma cell lines to retinoic acid. **Figure 5** shows the results from BE(2)-C cell treatment with 5 μM ATRA with neurite outgrowth images **(Figure 5A)**, analysis of neurite outgrowth **(Figure 5B)**, analysis of cell viability **(Figure 5C)**, and detection of molecular differentiation markers **(Figure 5D)**. There was a decrease in cell body area and an increase in neurite outgrowth **(Figure 5A)**, a significant increase in neurite outgrowth **(Figure 5B)**, and a significant reduction in cell viability **(Figure 5C)**. Following treatment with ATRA, there was also some over-expression of GAP43, a slight increase of expression in β(III) Tubulin, and a

slight under-expression of NSE **(Figure 5D).** Together, these analyses provide evidence for some cell differentiation in BE(2)-C cells following treatment with ATRA.

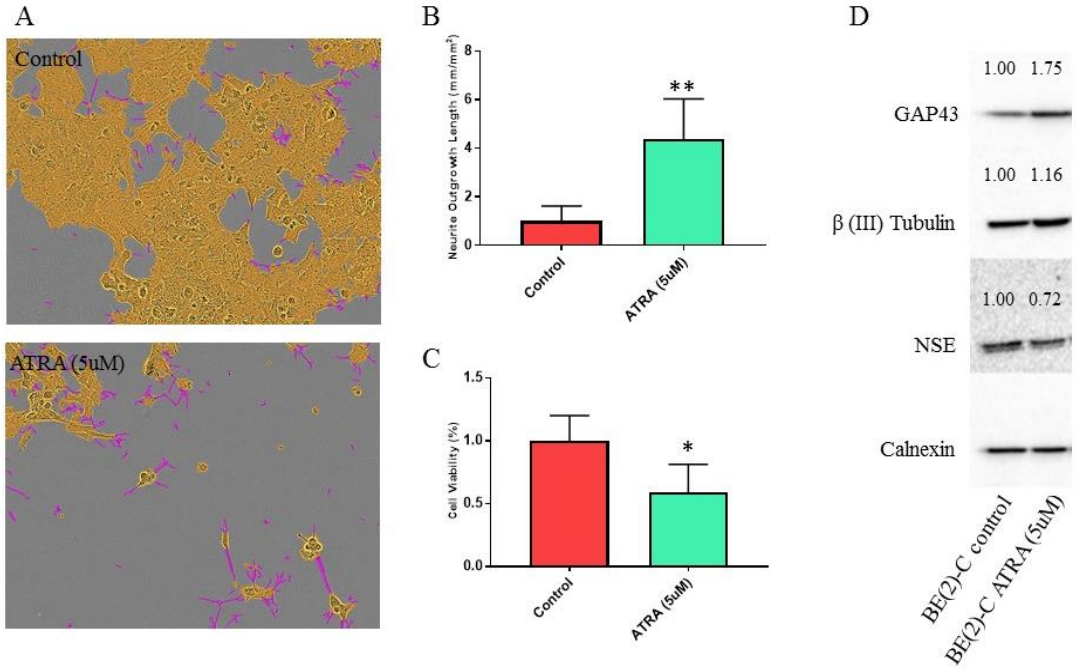

Figure 5. The Effect of ATRA in BE(2)-C Cells. (A) Neurite outgrowth images of control (top) and 5 μM ATRA treatment (bottom) of BE(2)-C cells taken at 20X magnification with cell body area (yellow) and neurite outgrowth (purple). (B) Statistical analysis of neurite outgrowth for control and ATRA treatment in BE(2)-C cells. (C) Statistical analysis of cell viability for control and ATRA treatment in BE(2)-C cells. (D) Quantification of molecular differentiation marker expression of Western Blots for control and ATRA treatment in BE(2)-C cells. Neurite outgrowth images are representative of nine non-overlapping individual images from a single sample. Error bars reflect SEM of n = 3 technical replicates; * $P \leq 0.05$, ** $P \leq 0.01$.

3.2.2 Kelly Cells

The next cell line to be tested were Kelly cells, which are known to be ATRA-resistant cells.[8] **Figure 6** shows the results from Kelly cell treatment with 5 μM ATRA with neurite outgrowth images **(Figure 6A)**, analysis of neurite outgrowth **(Figure 6B)**, analysis of cell viability **(Figure 6C)**, and detection of molecular differentiation markers **(Figure 6D)**. A slight decrease in cell body area and a slight an increase in neurite

outgrowth was observed **(Figure 6A)**, however there was not a statistically significant increase in neurite outgrowth **(Figure 6B)** or a statistically significant reduction in cell viability **(Figure 6C)** as observed in these figures. There was detectable increase in expression of all three molecular differentiation markers **(Figure 6D).** These results together confirm Kelly cells as an ATRA-resistant cell line as demonstrated by analyses of neurite outgrowth and viability, and indicate only slight differentiation of the cells by Western Blot.

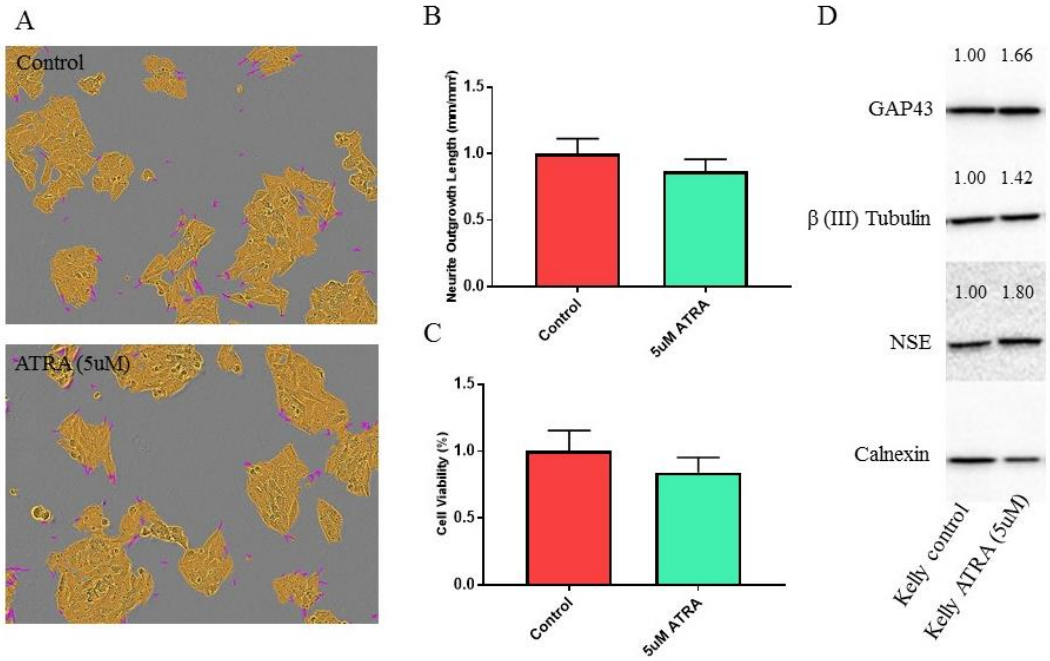

Figure 6. The Effect of ATRA in Kelly Cells. (A) Neurite outgrowth images of control (top) and 5 μM ATRA treatment (bottom) of Kelly cells taken at 20X magnification with cell body area (yellow) and neurite outgrowth (purple). (B) Statistical analysis of neurite outgrowth for control and ATRA treatment in Kelly cells. (C) Statistical analysis of cell viability for control and ATRA treatment in Kelly cells. (D) Quantification of molecular differentiation marker expression of Western Blots for control and ATRA treatment in Kelly cells. Neurite outgrowth images are representative of nine non-overlapping individual images from a single sample. Error bars reflect SEM of n = 3 technical replicates.

3.2.3 CHLA-90 Cells

Following treatment with ATRA in CHLA-90 cells, there was a significant increase in neurite outgrowth as observed in the neurite images **(Figure 7A)** and analysis **(Figure 7B)**. The viability of the ATRA-treated cells was reduced as compared to the control **(Figure 7C)**, and the presence of molecular differentiation markers was increased in treatment cells as compared to the control **(Figure 7D)**. All three analyses here support the conclusion that neuroblastoma cell differentiation did occur in CHLA-90 cells.

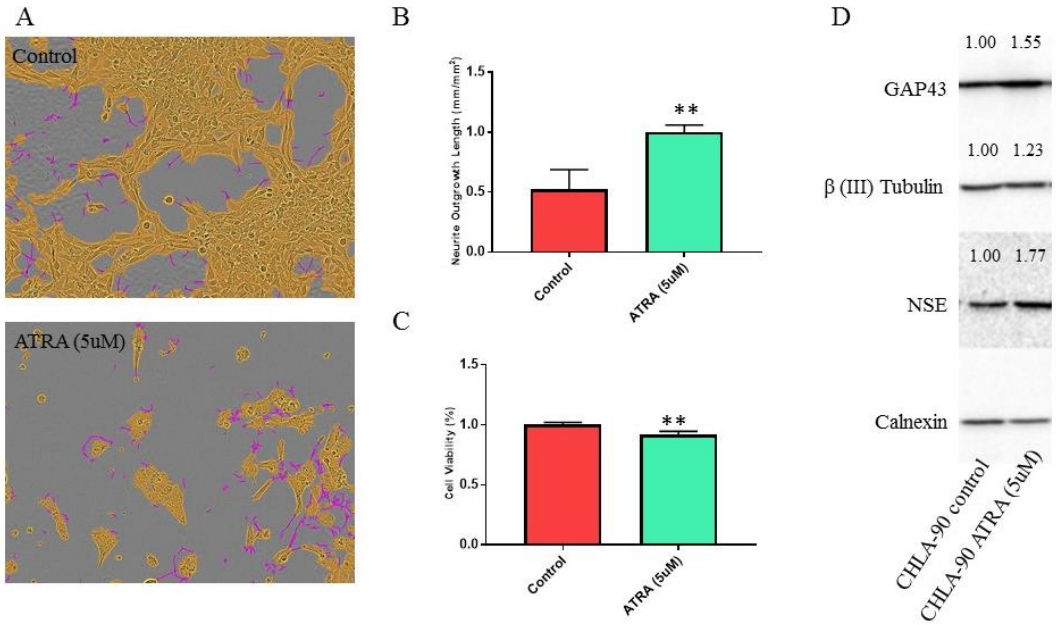

Figure 7. The Effect of ATRA in CHLA-90 Cells. (A) Neurite outgrowth images of control (top) and 5 μM ATRA treatment (bottom) of CHLA-90 cells taken at 20X magnification with cell body area (yellow) and neurite outgrowth (purple). (B) Statistical analysis of neurite outgrowth for control and ATRA treatment in CHLA-90 cells. (C) Statistical analysis of cell viability for control and ATRA treatment in CHLA-90 cells. (D) Quantification of molecular differentiation marker expression of Western Blots for control and ATRA treatment in CHLA-90 cells. Neurite outgrowth images are representative of nine non-overlapping individual images from a single sample. Error bars reflect SEM of n = 3 technical replicates; ** $P \leq 0.01$.

3.2.4 SK-N-DZ Cells

It has been established that some neuroblastoma cell lines grow spontaneous neurites in untreated cells, like SK-N-DZ and SK-N-F1 cells. This makes the molecular confirmation of differentiation more difficult in these cell lines, and one must provide convincing evidence to support this. For SK-N-DZ cells, it was determined that treatment with ATRA did produce cell differentiation as determined in **Figure 8**. The neurite images in **Figure 8A** shows a reduction in cell body area along with an increase in neurite outgrowth. However, the analyses of neurite outgrowth **(Figure 8B)** did not show a statistically significant increase. There is evidence of cell differentiation from the viability analysis **(Figure 8C)**, and an increase in two out of the three molecular differentiation markers as observed in **Figure 8D**. Although the neurite outgrowth does not provide significant evidence of cell differentiation, the viability and presence of differentiation markers suggest that SK-N-DZ cells did differentiate following ATRA treatment.

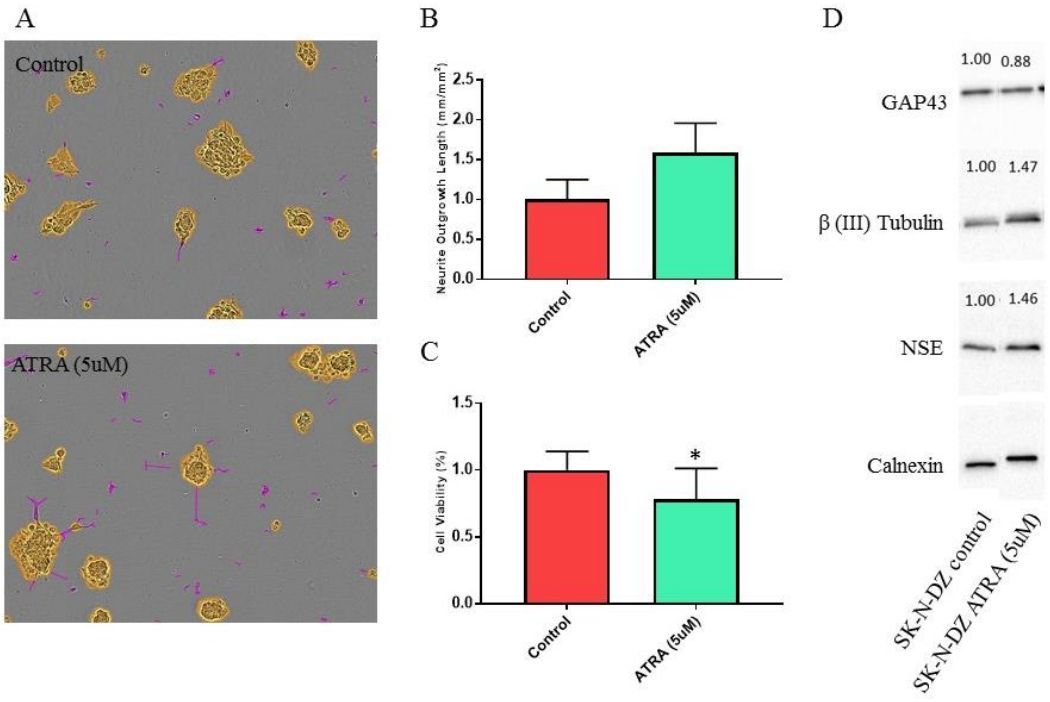

Figure 8. The Effect of ATRA in SK-N-DZ Cells. (A) Neurite outgrowth images of control (top) and 5 μM ATRA treatment (bottom) of SK-N-DZ cells taken at 20X magnification with cell body area (yellow) and neurite outgrowth (purple). (B) Statistical analysis of neurite outgrowth for control and ATRA treatment in SK-N-DZ cells. (C) Statistical analysis of cell viability for control and ATRA treatment in SK-N-DZ cells. (D) Quantification of molecular differentiation marker expression of Western Blots for control and ATRA treatment in SK-N-DZ cells. Neurite outgrowth images are representative of nine non-overlapping individual images from a single sample. Error bars reflect SEM of n = 3 technical replicates; * $P \leq 0.05$.

3.2.5 SK-N-F1 Cells

Figure 9 shows the results of ATRA treatment on SK-N-F1 cells and presents evidence of cell differentiation in two of the three analyses. The neurite outgrowth images in **Figure 9A** show spontaneous neurite outgrowth in control cells, as described above. There was significant neurite outgrowth as seen in **Figure 9B**, and increased expression of molecular differentiation markers **(Figure 9D)**. Despite this, there was not a significant reduction in cell viability for ATRA treated cells as compared to control cells **(Figure 9C)**.

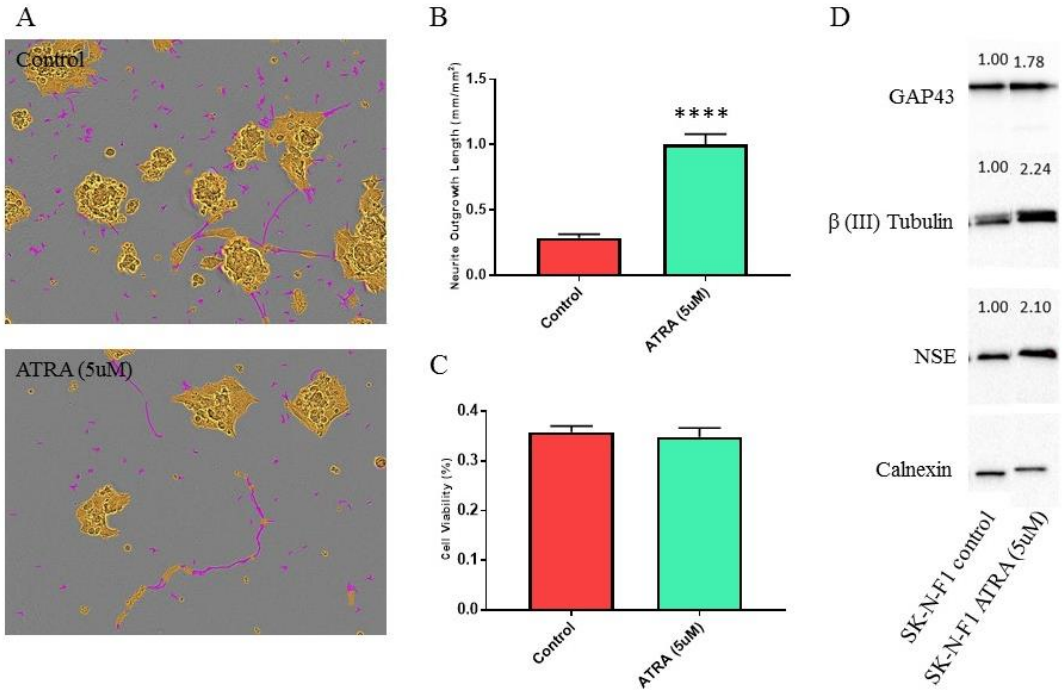

Figure 9. The Effect of ATRA in SK-N-F1 Cells. (A) Neurite outgrowth images of control (top) and 5 μM ATRA treatment (bottom) of SK-N-F1 cells taken at 20X magnification with cell body area (yellow) and neurite outgrowth (purple). (B) Statistical analysis of neurite outgrowth for control and ATRA treatment in SK-N-F1 cells. (C) Statistical analysis of cell viability for control and ATRA treatment in SK-N-F1 cells. (D) Quantification of molecular differentiation marker expression of Western Blots for control and ATRA treatment in SK-N-F1 cells. Neurite outgrowth images are representative of nine non-overlapping individual images from a single sample. Error bars reflect SEM of n = 3 technical replicates; **** $P \leq 0.0001$.

3.2.6 Summary of ATRA Treatment on 15 Neuroblastoma Cell Lines

The above analyses were performed in 10 more neuroblastoma cell lines as described in **Table 2**. This table shows evidence of neuroblastoma cell differentiation based on the neurite outgrowth increase relative to control and percent decrease in cell viability relative to control. There were seven cell lines that showed at statistically significant increase in neurite outgrowth and there were also eight cell lines that showed a

significant percent decrease in cell viability. Overall, these results indicated that some of the neuroblastoma cell lines are sensitive to ATRA-induced cell differentiation.

Table 2. Table of Neuroblastoma Cell Line Sensitivity to ATRA. Results for neurite outgrowth assays and cell viability assays for all 15 neuroblastoma cell lines treated with ATRA, showing the neurite outgrowth fold change, percent viability decrease, and statistical significance for control to ATRA treated cells. Statistical significance based on *P*-value, where $P \leq 0.05$ is considered statistically significant.

NB Cell Lines	ATRA (5uM)	
	N.O. fold change	% viability decrease
BE(2)-C	4.38*	41%*
Kelly	0.87	16%
CHLA-90	1.48*	8%
SK-N-DZ	1.58	22%*
SK-N-F1	1.29*	65%
SK-N-BE(2) [NS]	2.05	38%*
SK-N-AS [NS]	1.21	27%*
BE(2)-M17 [NS]	1.15	33%*
CHP-212 [NS]	2.19*	35%*
SH-SY5Y [NS]	0.64	3%
MC-IXC [NS]	1.76	56%*
IMR-32 [NS]	0.98	26%*
SK-N-MC [NS]	2.24*	53%*
SK-N-SH [NS]	1.27	3%
NGP [NS]	2.70*	43%*

3.3 Neuroblastoma Cell Lines with Different Genetic Backgrounds Show Varied Responses to Treatment with miR-506-3p Mimic

3.3.1 BE(2)-C Cells

To determine the miR-506-3p mimic effect on neuroblastoma cell differentiation, the next step in this project was to analyze the response of this mimic on the same neuroblastoma cell lines as described in **Figures 5-9** (i.e., BE(2)-C, Kelly, CHLA-90, SK-N-DZ, and SK-N-F1 cells). The first cell line was transfected with the miR-506-3p mimic at 2.5 nM and analyzed for neurite outgrowth and cell viability. **Figure 10** shows the results of these analyses, with neurite images **(Figure 10A)**, and statistical analyses **(Figure 10B and 10C)**. The statistical analyses for this experiment were consistent with the neurite images, showing a significant increase in neurite outgrowth following treatment with the mimic, and a significant reduction in cell viability. These results indicate a significant increase in cell differentiation in BE(2)-C cells following treatment.

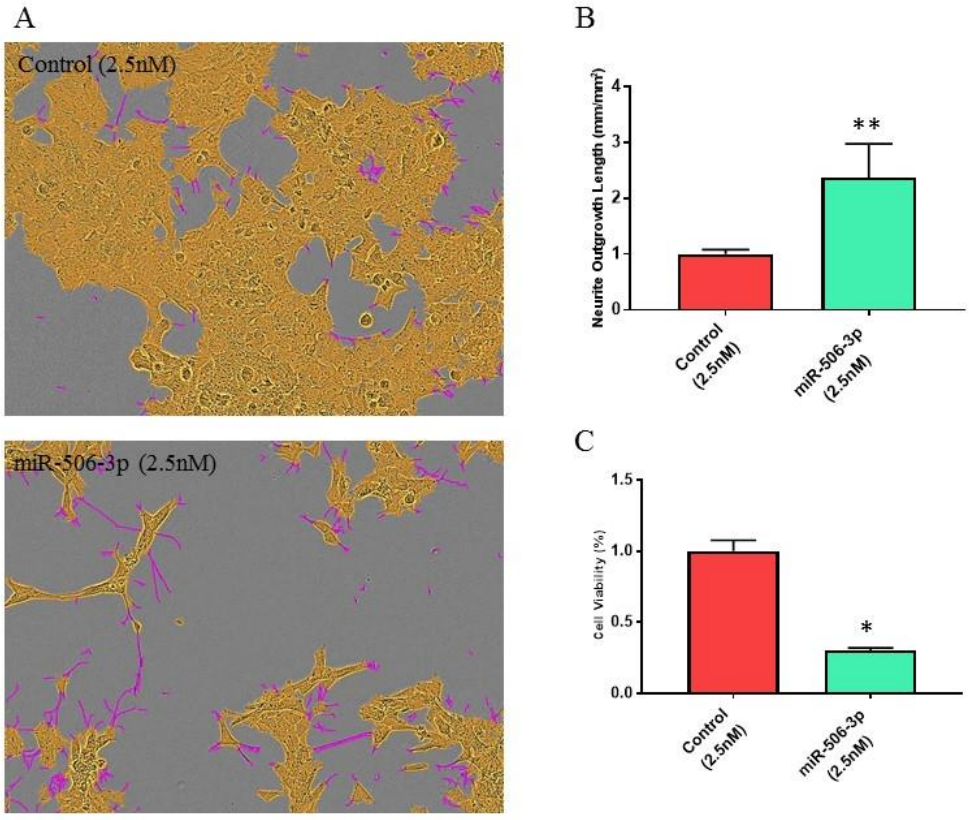

Figure 10. The Effect of miR-506-3p Mimic in BE(2)-C Cells. (A) Neurite outgrowth images of 2.5 nM control oligos (top) and 2.5 nM miR-506-3p mimic treatment (bottom) of BE(2)-C cells taken at 20X magnification with cell body area (yellow) and neurite outgrowth (purple). (B) Statistical analysis of neurite outgrowth for control and mimic treatment in BE(2)-C cells. (C) Statistical analysis of cell viability for control and mimic treatment in BE(2)-C cells. Neurite outgrowth images are representative of nine non-overlapping individual images from a single sample. Error bars reflect SEM of n = 3 technical replicates; * $P \leq 0.05$, ** $P \leq 0.01$.

Figure 10 shows another approach that was performed to analyze the long-term effect of the miR-506-3p mimic on cell proliferation in BE(2)-C cells. The results are observable in the scanned image in **Figure 11A**, showing a reduction in the number of colonies for the mimic-treated cells as compared to the control cells. Statistical analysis of this assay reveals that there was a significant reduction in the number of colonies after treatment with the mimic **(Figure 11B)**, but not a significant reduction in the average size

of the colonies **(Figure 11C)**. This may be due to two things, (1) the heterogeneous nature of neuroblastoma cells, such that the growth conditions and treatments can cause the cells to grow differently (as mentioned previously), and (2) there can only be two outcomes from treatment with the miR-506-3p mimic (i.e., cell death or no effect).

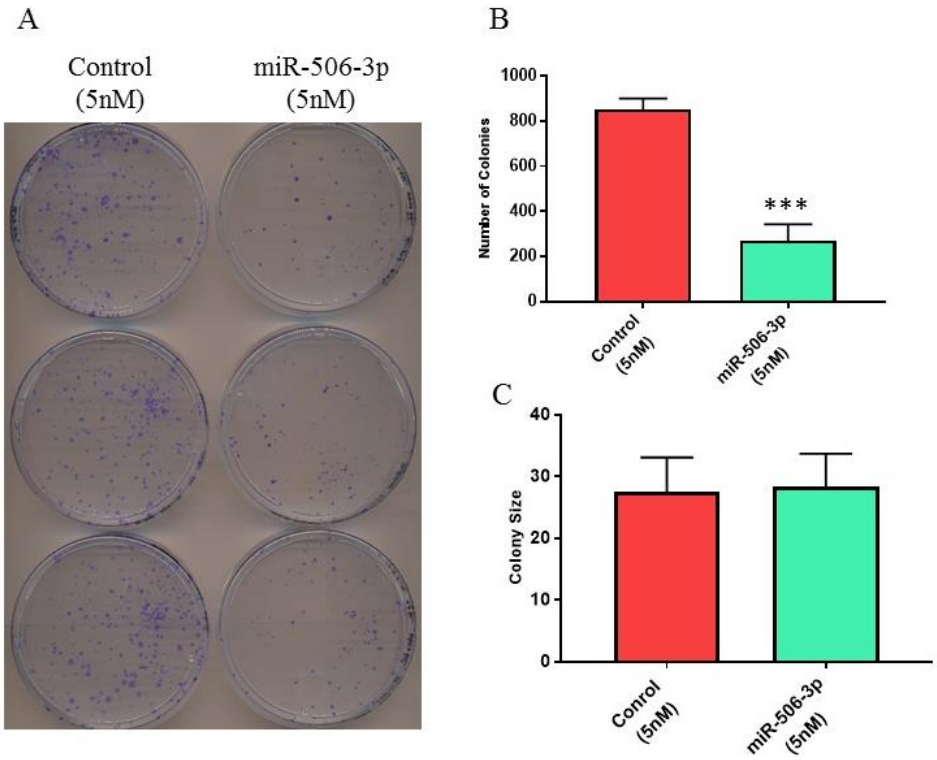

Figure 11. The Effect of miR-506-3p Mimic on Cell Proliferation in BE(2)-C Cells. (A) Scanned image of 5 nM control oligos (left) and 5 nM miR-506-3p mimic treatment (right) of BE(2)-C plated cells showing colonies formed (purple). (B) Statistical analysis of the number of colonies for control and mimic treatment in BE(2)-C cells. (C) Statistical analysis of the average colony size for control and mimic treatment in BE(2)-C cells. Error bars reflect SEM of n = 3 technical replicates; *** $P \leq 0.001$.

3.3.2 Kelly Cells

Figure 12 shows the result of Kelly cells treated with the miR-506-3p mimic from both a neurite outgrowth assay and a cell viability assay. The images in **Figure 12A** show a reduction in cell body area and an increase in neurite outgrowth for the mimic-treated cells as compared to the control, and the statistical analyses in **Figure 12B** show a slight increase in neurite outgrowth and a significant reduction in cell viability **(Figure 12C)**. These results indicate increased differentiation of Kelly cells, following treatment with the miR-506-3p mimic.

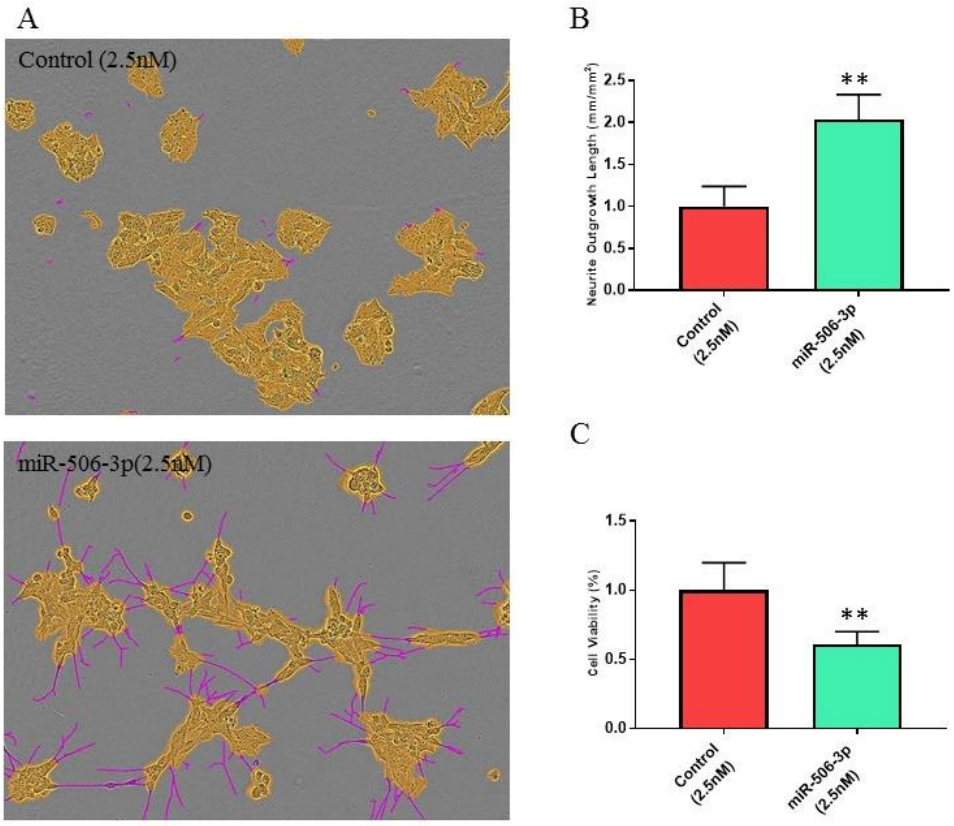

Figure 12. The Effect of miR-506-3p Mimic in Kelly Cells. (A) Neurite outgrowth images of 2.5 nM control oligos (top) and 2.5 nM miR-506-3p mimic treatment (bottom) of Kelly cells taken at 20X magnification with cell body area (yellow) and neurite outgrowth (purple). (B) Statistical analysis of neurite outgrowth for control and mimic treatment in Kelly cells. (C) Statistical analysis of cell viability for control and mimic treatment in Kelly cells. Neurite outgrowth images are representative of nine non-overlapping individual images from a single sample. Error bars reflect SEM of n = 3 technical replicates; ** $P \leq 0.01$.

The conclusion that miR-506-3p mimic treatment induced cell differentiation in Kelly cells, was confirmed in **Figure 13** with a cell proliferation assay. **Figure 13A** shows the scanned image of these cells after treatment with 5 nM miR-506-3p mimic. The image shows a decrease in the number of colonies between the control and mimic-treated cells, which is confirmed in the statistical analysis in **Figure 13B**. As previously seen in BE(2)-C cells **(Figure 11C)**, there is no significant difference in the average sizes

of the colonies **(in Figure 13C)** due to the effect of the mimic on the cells and the heterogeneous nature of neuroblastoma cells.

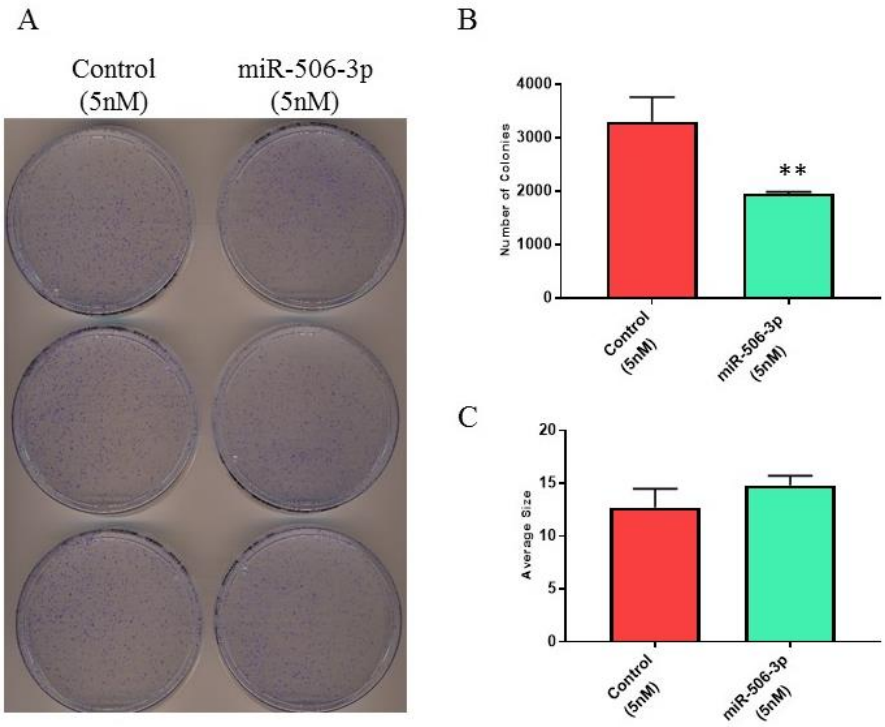

Figure 13. The Effect of miR-506-3p Mimic on Cell Proliferation in Kelly Cells. (A) Scanned image of 5 nM control oligos (left) and 5 nM miR-506-3p mimic treatment (right) of Kelly plated cells showing colonies formed (purple). (B) Statistical analysis of the number of colonies for control and mimic treatment in Kelly cells. (C) Statistical analysis of the average colony size for control and mimic treatment in Kelly cells. Error bars reflect SEM of n = 3 technical replicates; ** $P \leq 0.01$.

3.3.3 CHLA-90 Cells

Figure 14 shows the results from treating CHLA-90 cells with the miR-506-3p mimic for neurite outgrowth and cell viability. The results in **Figure 14B** show a highly significant increase in neurite outgrowth for treated cells versus control cells, as determined by the neurite outgrowth assay **Figure 14A**. **Figure 14C** presents the

statistical significance of reduction in viability for the mimic-treated cells. These results together indicate that the miR-506-3p mimic induced differentiation in CHLA-90 cells.

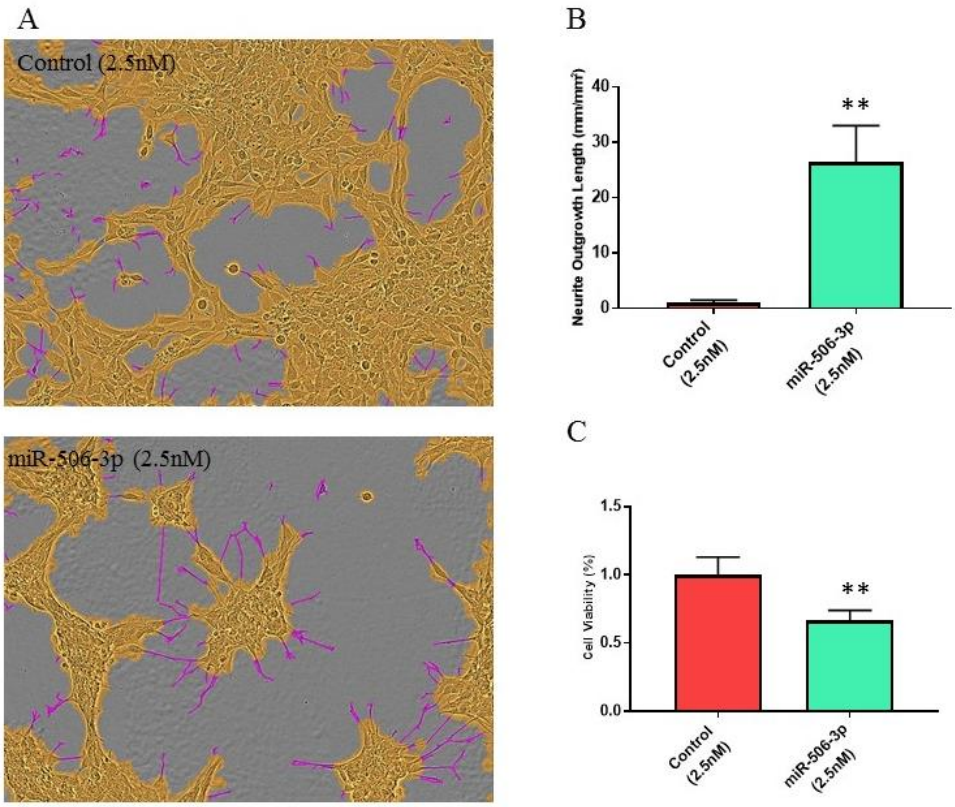

Figure 14. The Effect of miR-506-3p Mimic in CHLA-90 Cells. (A) Neurite outgrowth images of 2.5 nM control oligos (top) and 2.5 nM miR-506-3p mimic treatment (bottom) of CHLA-90 cells taken at 20X magnification with cell body area (yellow) and neurite outgrowth (purple). (B) Statistical analysis of neurite outgrowth for control and mimic treatment in CHLA-90 cells. (C) Statistical analysis of cell viability for control and mimic treatment in CHLA-90 cells. Neurite outgrowth images are representative of nine non-overlapping individual images from a single sample. Error bars reflect SEM of n = 3 technical replicates; ** $P \leq 0.01$.

To support this conclusion, a colony formation assay was performed to measure the effect of the miR-506-3p mimic on CHLA-90 cell proliferation. The image in **Figure 15A** shows a decrease in the number of colonies for mimic-treated cells when compared to control cells, which is consistent with the results in **Figure 15B** indicated by the

statistical significance for the mimic-treated cells. In contrast, there was not a significant change in the average size of the colonies between treatments **(Figure 15C)**, as is consistent with the cell lines mentioned above **(Figure 11C and 13C).** These results indicate this experiment should be repeated with less cells for accurate determination of miR-506-3p mimic effect on cell proliferation in CHLA-90 cells.

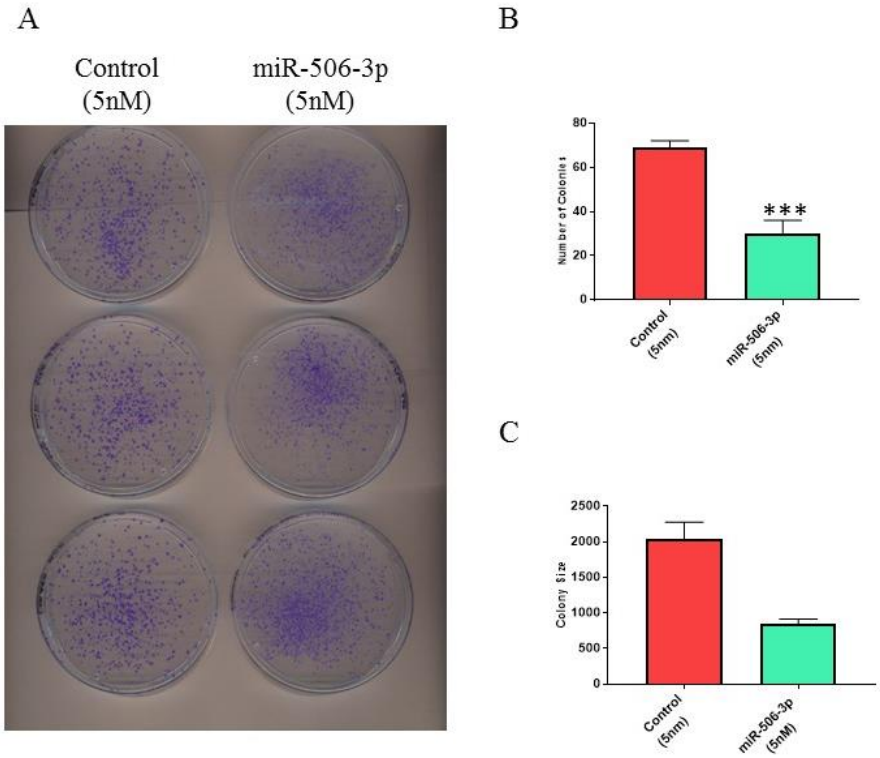

Figure 15. The Effect of miR-506-3p Mimic on Cell Proliferation in CHLA-90 Cells. (A) Scanned image of 5 nM control oligo (left) and 5 nM miR-506-3p mimic treatment (right) of CHLA-90 plated cells showing colonies formed (purple). (B) Statistical analysis of the number of colonies for control and mimic treatment in CHLA-90 cells. (C) Statistical analysis of the average colony size for control and mimic treatment in CHLA-90 cells. Error bars reflect SEM of n = 3 technical replicates; *** $P \leq 0.001$.

3.3.4 SK-N-DZ Cells

The next cell line analyzed for the response to treatment with the miR-506-3p mimic was SK-N-DZ cells. **Figure 16** shows the results of these analyses, with neurite images for the control versus mimic-treated cells **(Figure 16A)**, statistical analysis of neurite outgrowth **(Figure 16B)**, and statistical analysis of the cell viability **(Figure 16C)**. There was a significant increase in the neurite outgrowth following mimic treatment **(Figure 16B)**, but there was a very significant reduction in viability showing over 50% reduction of the cells **(Figure 16C)**. Due to the strong reduction in cell viability, it is conclusive that the miR-506-3p mimic induces cell differentiation in the SK-N-DZ cells.

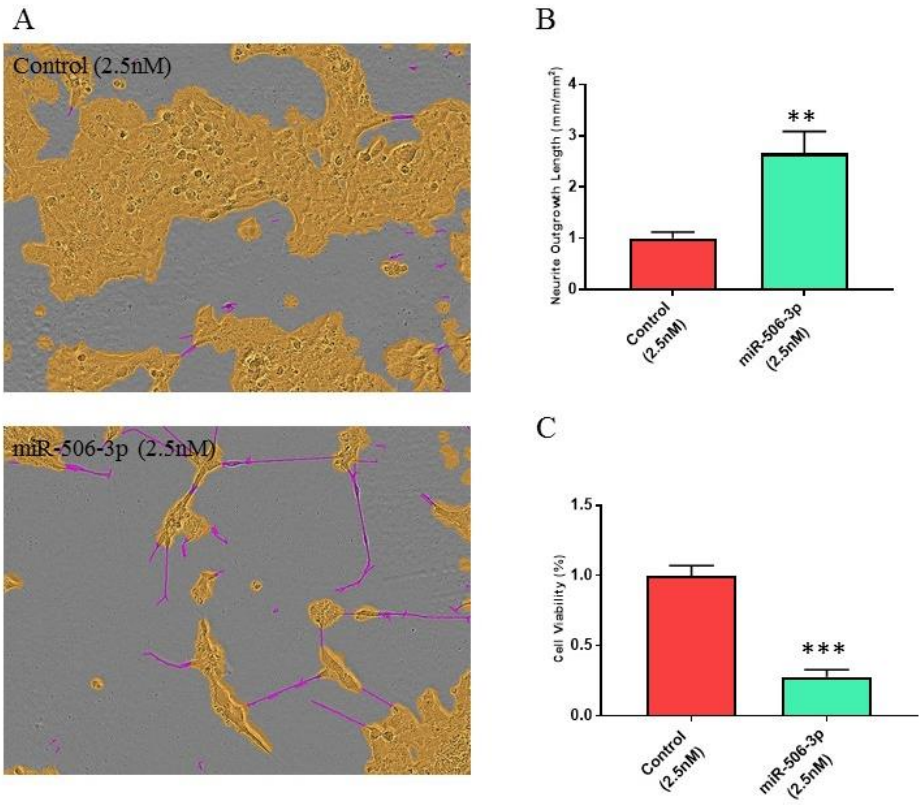

Figure 16. The Effect of miR-506-3p Mimic in SK-N-DZ Cells. (A) Neurite outgrowth images of 2.5 nM control oligos (top) and 2.5 nM miR-506-3p mimic treatment (bottom) of SK-N-DZ cells taken at 20X magnification with cell body area (yellow) and neurite outgrowth (purple). (B) Statistical analysis of neurite outgrowth for control and mimic treatment in SK-N-DZ cells. (C) Statistical analysis of cell viability for control and mimic treatment in SK-N-DZ cells. Neurite outgrowth images are representative of nine non-overlapping individual images from a single sample. Error bars reflect SEM of n = 3 technical replicates; ** $P \leq 0.01$, *** $P \leq 0.001$.

3.3.5 SK-N-F1 Cells

The final cell line analyzed for cell differentiation following treatment with the miR-506-3p mimic, was the SK-N-F1 cell line as shown in **Figure 17**. The neurite images show a reduction in the cell body area and an increase in the neurite outgrowth **(Figure 17A)**, as confirmed by the analysis in **Figure 17B**, which shows a significant increase in neurite outgrowth for mimic-treated cells versus control cells. The cell

viability analysis did not show a significant reduction in the mimic-treated cells **(Figure 17C)**, indicating that this experiment needs to be repeated for accurate determination of cell differentiation in SK-N-F1 cells.

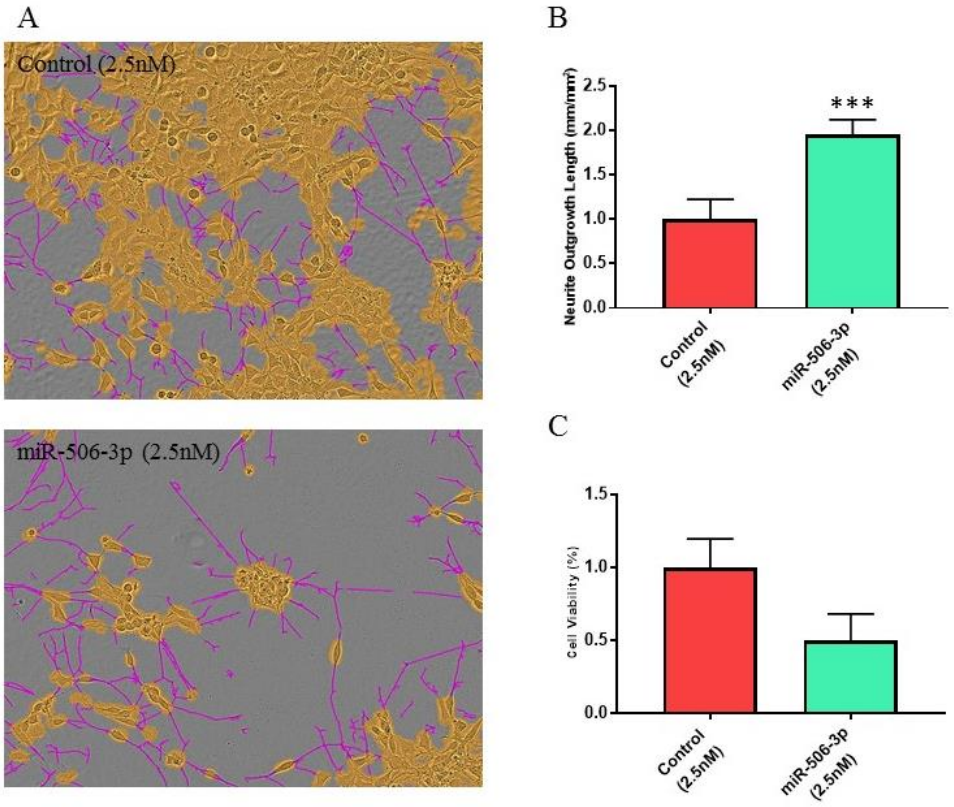

Figure 17. The Effect of miR-506-3p Mimic in SK-N-F1 Cells. (A) Neurite outgrowth images of 2.5 nM control oligos (top) and 2.5 nM miR-506-3p mimic treatment (bottom) of SK-N-F1 cells taken at 20X magnification with cell body area (yellow) and neurite outgrowth (purple). (B) Statistical analysis of neurite outgrowth for control and mimic treatment in SK-N-F1 cells. (C) Statistical analysis of cell viability for control and mimic treatment in SK-N-F1 cells. Neurite outgrowth images are representative of nine non-overlapping individual images from a single sample. Error bars reflect SEM of n = 3 technical replicates; *** $P \leq 0.001$.

3.3.6 Summary of miR-506-3p Mimic Treatment on 5 Neuroblastoma Cell Lines

To summarize these results, **Table 3** provides a quantitative analysis of the results mentioned above for miR-506-3p mimic treatment on five neuroblastoma cell lines. The table shows the fold change for neurite outgrowth, the percent decrease on cell viability, and the ratio of the fold change for the number of colonies with the cell proliferation assay. All these analyses are based on treatment versus control groups, where the table shows a significant increase in neurite outgrowth and a significant decrease in percent viability for all cell lines tested. The table also shows statistical significance in all cell lines tested for the ratio of the fold change in the number of colonies by the cell proliferation assays. These results provide evidence for miR-506-3p as a differentiation-inducing agent in neuroblastoma cells.

Table 3. Table of Neuroblastoma Cell Line Sensitivity to miR-506-3p Mimic. Results for neurite outgrowth assays and cell viability assays for five neuroblastoma cell lines treated with the miR-506-3p mimic, showing the neurite outgrowth fold change, percent viability decrease, percent cell proliferation decrease, and the statistical significance for control to mimic-treated cells. *Statistical significance based on *P*-value, where $P \leq 0.05$ is considered statistically significant.

NB Cell Lines	MiR-506-3p Mimic (2.5nM)		MiR-506-3p Mimic (5nM)
	N.O. fold change	% viability decrease	% cell proliferation decrease
BE(2)-C	2.37*	70%*	68%*
Kelly	2.04*	39%*	41%*
CHLA-90	26.39*	17%*	44%*
SK-N-DZ	2.65*	72%*	n/a
SK-N-F1	1.95*	50%*	n/a

3.3.7 Summary of Neuroblastoma Cell Lines Showing Differential Responses to Treatment with ATRA and the miR-506-3p Mimic

The last step of the first aim was to determine the correlation between ATRA and the miR-506-3p mimic sensitivity in neuroblastoma cells. **Table 4** summarizes the analyses of ATRA treatment versus miR-506-3p mimic treatment on neuroblastoma cell lines, in which the sensitivity to treatment was based on P-values, with $P < 0.05$ considered significant. These results indicate that miR-506-3p mimic induced differentiation in all five cell types, while ATRA only conclusively induced differentiation in two types (i.e., BE(2)-C and CHLA-90 cells).

Table 4. Table Showing the Correlation Between Neuroblastoma Cell Line Sensitivity to ATRA and miR-506-3p Mimic. Results for neurite outgrowth assays and cell viability assays for all 15 neuroblastoma cell lines treated with ATRA or the miR-506-3p mimic. This comparison is a non-quantitative analysis reporting sensitivity to treatment based off *P*-values, with $P \leq 0.05$ considered significant and therefore sensitive to the treatment.

NB Cell Lines	ATRA (5uM)		MiR-506-3p Mimic (2.5nM)	
	Neurite outgrowth	Cell viability	Neurite outgrowth	Cell viability
BE(2)-C	sensitive	sensitive	sensitive	sensitive
Kelly	non-sensitive	non-sensitive	sensitive	sensitive
CHLA-90	sensitive	sensitive	sensitive	sensitive
SK-N-DZ	non-sensitive	sensitive	sensitive	sensitive
SK-N-F1	sensitive	non-sensitive	sensitive	sensitive
SK-N-BE(2)	non-sensitive	sensitive		
SK-N-AS	non-sensitive	sensitive		
BE(2)-M17	non-sensitive	sensitive		
CHP-212	sensitive	sensitive		
SH-SY5Y	non-sensitive	non-sensitive		
MC-IXC	non-sensitive	sensitive		
IMR-32	non-sensitive	sensitive		
SK-N-MC	sensitive	sensitive		
SK-N-SH	non-sensitive	non-sensitive		
NGP	sensitive	sensitive		

3.4 Combined ATRA and miR-506-3p Mimic Treatments Do Not Show a Synergistic Effect on Cell Survival in Neuroblastoma Cell Lines

The second aim of the project was to determine if the combined treatment with ATRA and the miR-506-3p mimic synergistically promoted neuroblastoma cell differentiation. A synergistic effect of two treatments means that the combined effect of two agents was greater than the sum of the effects of the individual agents. The two alternatives to a synergistic effect are either an additive effect, in which the combination treatment yields that equals the sum of the individual agents, or an antagonistic effect, in which the combination treatment outcome is reduced relative to the sum of the individual agent treatments.

As described above, the two established assays for differentiation are neurite outgrowth and cell viability via MTT assay. There are no current methods available to quantitatively predict treatment additivity in neurite outgrowth assays, and so this assay is only able to qualitatively report on dual treatments. In contrast, synergism in cell viability assays can be robustly predicted and measured using the Bliss Independence Model, which is an established approach to calculate the predicted additivity of a combination of two drugs on cell viability.[50, 51] The Bliss Independence model defines the predicted additivity of a combination of two drugs with the formula

$$E_{xy,PA} = E_x + E_y - E_xE_y$$

where E_x and E_y are the effects of individual treatments *x* and *y*, E_xE_y is the product of the individual effects, and $E_{xy,PA}$ is the predicted additivity.[50, 51] The $E_{xy,PA}$ value is compared

to the experimental outcome of the dual treatment, $E_{xy,exp}$, to determine whether the dual treatment is synergistic, additive, or antagonistic.

Figure 18 demonstrates how this model is used. All samples are normalized to a control treatment (E = 1.0), in which 100% of the cells are viable. In this example, the normalized ATRA treatment effect is 0.7, with 70% of the cells viable and 30% of the cells killed by the treatment. The miR-506-3p mimic treatment produced an effect of 0.5, in which 50% of the cells survived and 50% of the cells were killed. In the Bliss model, the predicted additivity $E_{xy,PA} = 0.7 + 0.5 - (0.7 * 0.5) = 0.35$. In other words, assuming the two treatments are purely additive (i.e. not synergistic or antagonistic), 35% of the cells are expected to survive the dual treatment and 65% are predicted to die. When the experiment was carried out, the observed effect of combined treatment, $E_{xy,exp}$, was measured to be 0.15, reflecting 15% cell viability and 85% cell death. Because $E_{xy,exp}$ is less than $E_{xy,PA}$ ($0.15 < 0.35$), these data indicate that the combined treatment is synergistic. **Table 5** summarizes the predicted and experimental outcomes in terms of survival percentages, which is simply $100*E_{xy,PA}$ and $100*E_{xy,exp}$, respectively.

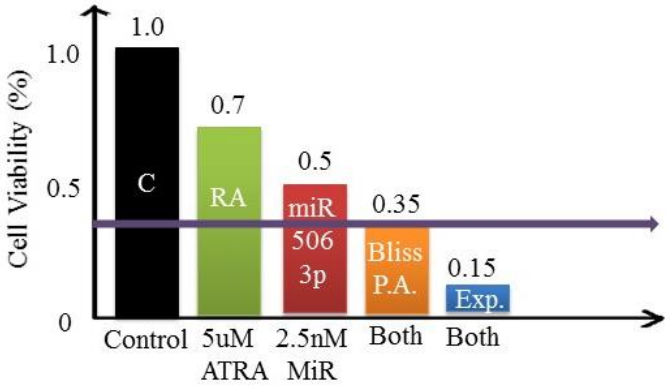

Figure 18. The Bliss Independence Model for Predicted Additivity. This figure represents a schematic showing different experimental treatments along with the Bliss Independence predicted additivity value used to compare to the combined treatment experimental value to determine synergy on cell viability.

3.4.1 BE(2)-C Cells

Using this model, the effect of combined treatment with ATRA and the miR-506-3p mimic was evaluated on the five neuroblastoma cell lines examined above. **Figure 19** shows the neurite images **(Figure 19A)** and the cell viability analysis **(Figure 19B)** for BE(2)-C cells. Consistent with the images in **Figure 19A**, the cell viability shows a significant reduction in cell survival for all treatments, including ATRA, miR-506-3p mimic, and the combined treatment. As expected from the individual treatments, these results indicate differentiation of the BE(2)-C cells.

To determine if the combined treatment had a synergistic or additive effect on cell viability, the Bliss Independence model was performed to calculate the predicted additivity. As shown in **Figure 19B**, the experimental value for combined treatment is greater than the predicted additivity value, indicating an enhanced but not synergistic effect from the combined treatment of ATRA and the miR-506-3p mimic on BE(2)-C cells.

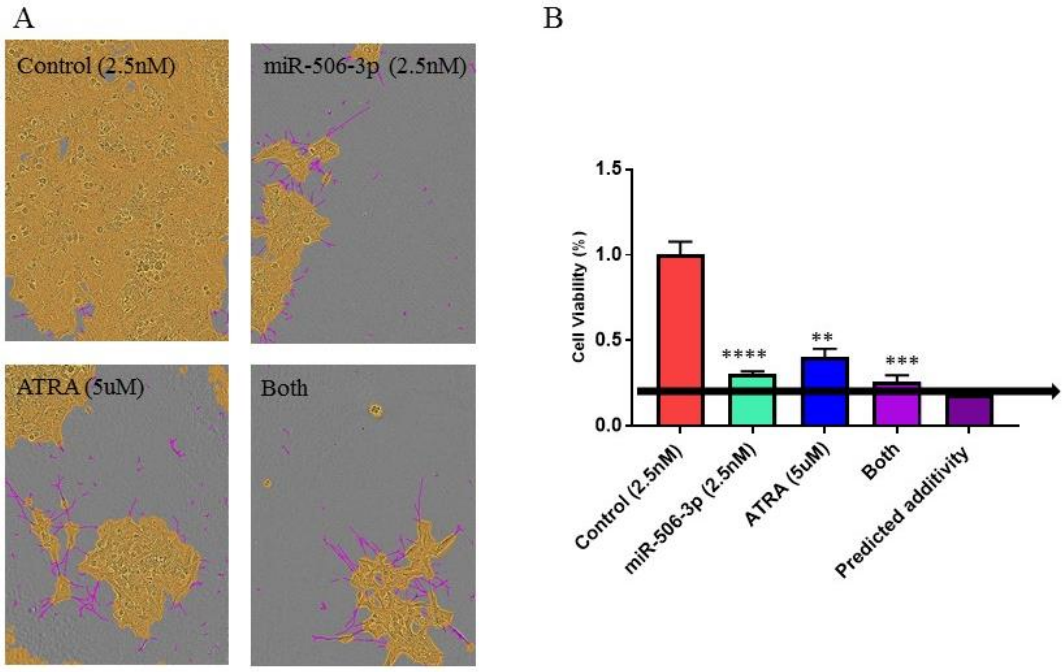

Figure 19. The Effect of Combined Treatment of ATRA and miR-506-3p Mimic in BE(2)-C Cells. (A) Neurite outgrowth images of 2.5 nM control oligos (top left), 2.5 nM miR-506-3p mimic (top right), 5 μM ATRA (bottom left), and combined treatments (bottom right) of BE(2)-C cells taken at 20X magnification with cell body area (yellow) and neurite outgrowth (purple). (B) Statistical analysis of cell viability for the mimic, ATRA, and combined treatments in BE(2)-C cells relative to the control, along with the calculated predicted additivity. Neurite outgrowth images are representative of nine non-overlapping individual images from a single sample. Error bars reflect SEM of n = 3 technical replicates; ** $P \leq 0.01$, *** $P \leq 0.001$, **** $P \leq 0.0001$.

3.4.2 Kelly Cells

For Kelly cells, there was a significant reduction in the cell survival for mimic-treated cells along with the combined treatment, but not for ATRA treatment in **Figure 20**. This is consistent with the results described in **Figure 6**, indicating a resistance to ATRA. The neurite images in **Figure 20A** are consistent with these results showing a slight decrease in the cell body area and increase in the neurite length for ATRA treatment, but show a statistically significant change for the mimic and combined treatments. **Figure 20B** does not show a synergistic effect from combined treatment with

ATRA and the miR-506-3p mimic, indicated by the experimental value being greater than the predicted additivity.

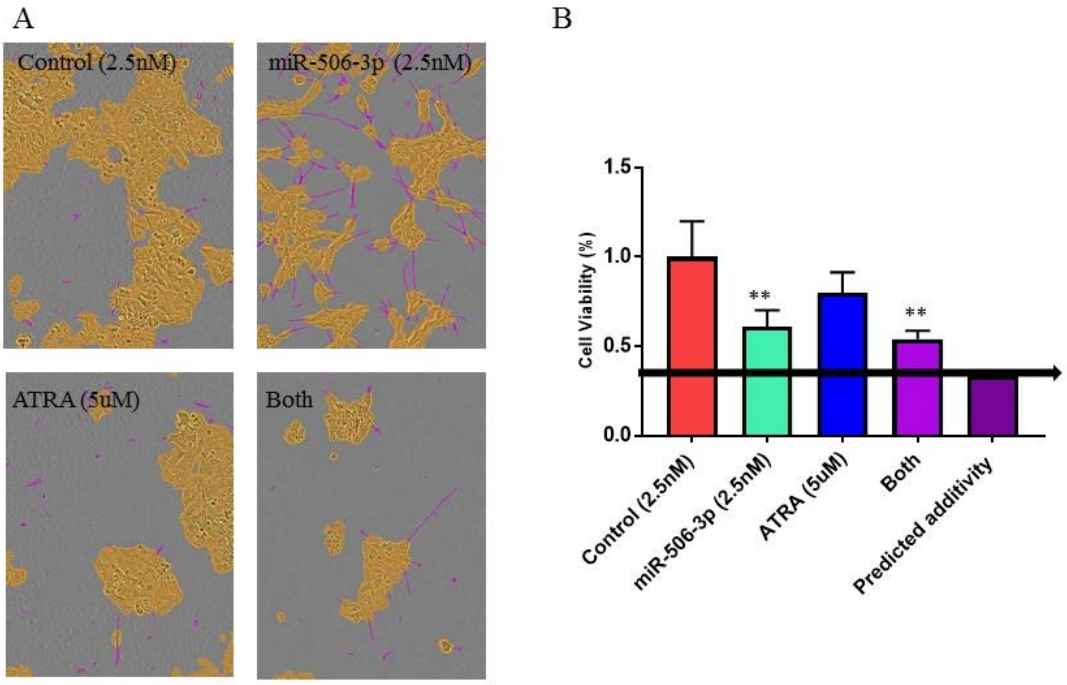

Figure 20. The Effect of Combined Treatment of ATRA and miR-506-3p Mimic in Kelly Cells. (A) Neurite outgrowth images of 2.5 nM control oligos (top left), 2.5 nM miR-506-3p mimic (top right), 5 µM ATRA (bottom left), and combined treatments (bottom right) of Kelly cells taken at 20X magnification with cell body area (yellow) and neurite outgrowth (purple). (B) Statistical analysis of cell viability for the mimic, ATRA, and combined treatments in Kelly cells relative to the control, along with the calculated predicted additivity. Neurite outgrowth images are representative of nine non-overlapping individual images from a single sample. Error bars reflect SEM of n = 3 technical replicates; ** $P \leq 0.01$.

3.4.3 CHLA-90 Cells

Figure 21 shows the effect of combined treatments on CHLA-90 cells. The neurite images in **Figure 21A** show a slight reduction in cell body area for mimic treatment and a more defined reduction in cell body area for the ATRA and combined

treatments, but an increase in neurite outgrowth is evident for all three treatment groups. The cell viability analysis **(Figure 21B)** shows statistical significance for the reduction in cell survival for all three treatments as compared to the control, but did not indicate a synergistic effect from the combined treatment on CHLA-90 cells.

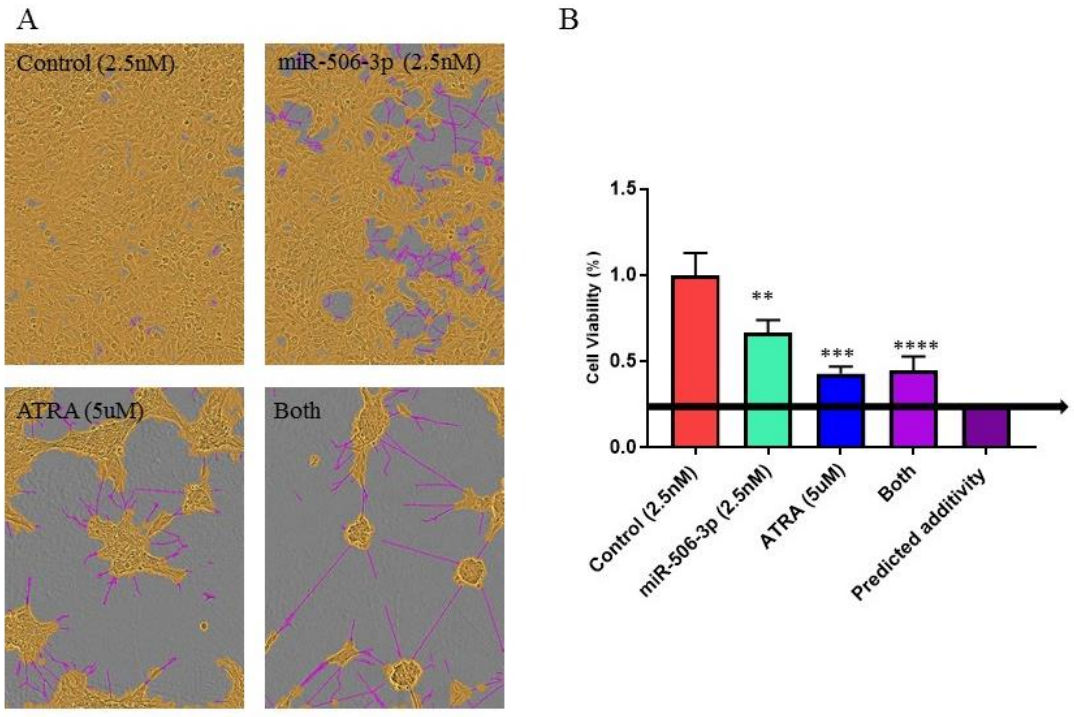

Figure 21. The Effect of Combined Treatment of ATRA and miR-506-3p Mimic in CHLA-90 Cells. (A) Neurite outgrowth images of 2.5 nM control oligos (top left), 2.5 nM miR-506-3p mimic (top right), 5 µM ATRA (bottom left), and combined treatments (bottom right) of CHLA-90 cells taken at 20X magnification with cell body area (yellow) and neurite outgrowth (purple). (B) Statistical analysis of cell viability for the mimic, ATRA, and combined treatments in CHLA-90 cells relative to the control, along with the calculated predicted additivity. Neurite outgrowth images are representative of nine non-overlapping individual images from a single sample. Error bars reflect SEM of n = 3 technical replicates; ** $P \leq 0.01$, *** $P \leq 0.001$, **** $P \leq 0.0001$.

3.4.4 SK-N-DZ Cells

For SK-N-DZ cells, **Figure 22** shows the effect of combined treatment of ATRA and the miR-506-3p mimic on cell viability. **Figure 22A** shows a decrease in cell body area and an increase in neurite outgrowth for all three treatment groups, with the most evident results for the mimic and combined treatment groups. Neurite outgrowth is consistent with cell viability as shown in **Figure 22B**. The graph shows a greater experimental value from combined treatment as compared to the predicted additivity, indicating there was not a synergistic effect on viability of combined treatment in SK-N-DZ cells.

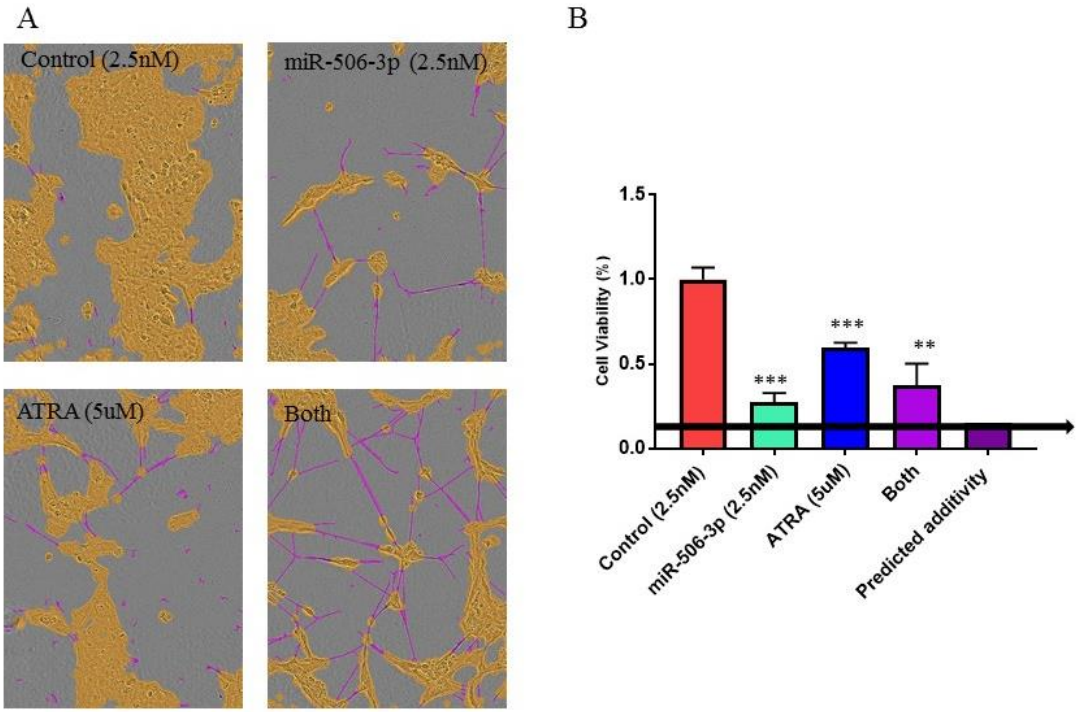

Figure 22. The Effect of Combined Treatment of ATRA and miR-506-3p Mimic in SK-N-DZ Cells. (A) Neurite outgrowth images of 2.5 nM control oligos (top left), 2.5 nM miR-506-3p mimic (top right), 5 µM ATRA (bottom left), and combined treatments (bottom right) of SK-N-DZ cells taken at 20X magnification with cell body area (yellow) and neurite outgrowth (purple). (B) Statistical analysis of cell viability for the mimic, ATRA, and combined treatments in SK-N-DZ cells relative to the control, along with the calculated predicted additivity. Neurite outgrowth images are representative of nine non-overlapping individual images from a single sample. Error bars reflect SEM of n = 3 technical replicates; ** $P \leq 0.01$, *** $P \leq 0.001$.

3.4.5 SK-N-F1 Cells

The results for the final cell line tested for the effect of combined treatment of ATRA and the miR-506-3p mimic on neuroblastoma cell viability is shown in **Figure 23**. All treated SK-N-F1 cells show a clear reduction in the cell body area and increase in the neurite outgrowth as observed in the neurite images in **Figure 23A**. **Figure 23B** shows the statistical analysis of cell viability on SK-N-F1 cells following treatment with the miR-506-3p mimic, ATRA, and combined treatment. There is a significant reduction in all three treatment groups as compared to the control on cell survival, but there was no indicated synergistic effect on cell viability for SK-N-F1 cells.

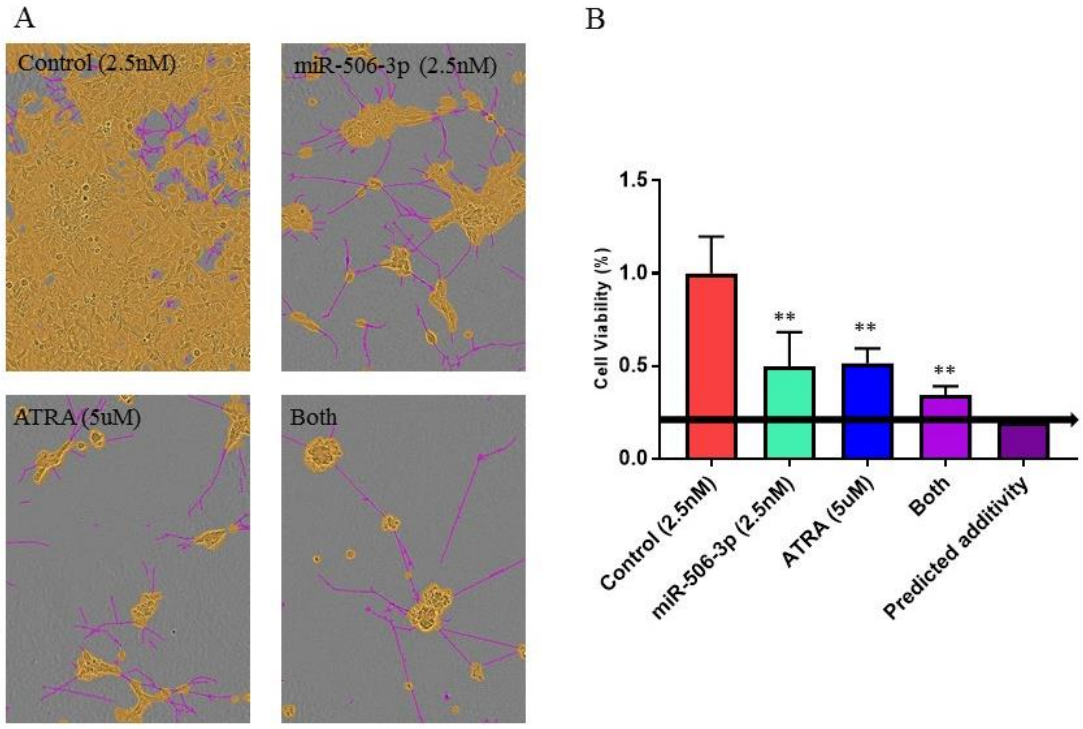

Figure 23. The Effect of Combined Treatment of ATRA and miR-506-3p Mimic in SK-N-F1 Cells. (A) Neurite outgrowth images of 2.5 nM control oligos (top left), 2.5 nM miR-506-3p mimic (top right), 5 µM ATRA (bottom left), and combined treatments (bottom right) of SK-N-F1 cells taken at 20X magnification with cell body area (yellow) and neurite outgrowth (purple). (B) Statistical analysis of cell viability for the mimic, ATRA, and combined treatments in SK-N-F1 cells relative to the control, along with the calculated predicted additivity. Neurite outgrowth images are representative of nine non-overlapping individual images from a single sample. Error bars reflect SEM of n = 3 technical replicates; ** $P \leq 0.01$.

3.4.6 Summary of Combined ATRA and miR-506-3p Mimic Treatments on Neuroblastoma Cell Viability

Table 5 shows the effect of combined treatment with ATRA and the miR-506-3p mimic on neuroblastoma cells with the percent survival of predicted additivity and the percent survival of experimental outcomes. The table combines the evidence from above **(Figures 19-23)** and does not indicate synergism due to the combined treatments for all cell lines reporting an experimental value greater than the predicted survival rates.

Table 5. Table of Neuroblastoma Cell Line Sensitivity to Combined Treatment of ATRA and miR-506-3p Mimic. Results for cell viability assays in 5 neuroblastoma cell lines treated with a combination of ATRA and the miR-506-3p mimic, showing the percent survival for the predicted and experimental treatments, and the observed effect. ↑ indicates an enhanced observed effect following treatment. *The observed effect was solely based on experimental values being compared to the predicted survival values; statistics remain to be performed.

Cell Lines	Combined Treatment (5uM ATRA and 2.5nM miR-506-3p)		
	% Survival, Predicted	% Survival, Experimental	Observed Effect*
BE(2)-C	56%	26%	↑
Kelly	73%	54%	↑
CHLA-90	56%	34%	↑
SK-N-DZ	49%	28%	↑
SK-N-F1	40%	85%	↑

IV. SUMMARY AND CONCLUSIONS

The main aims of this project were to determine the correlation of neuroblastoma cell sensitivity to retinoic acid and the miR-506-3p mimic, and to determine the effect of combined treatment with ATRA and the miR-506-3p mimic on neuroblastoma cell viability. The first aim required several steps, including determining the response to ATRA in neuroblastoma cell lines, determining the response to the miR-506-3p mimic in the same neuroblastoma cell lines, and determining the correlation between ATRA and the miR-506-3p mimic sensitivity. The second aim was to determine if the combined treatment of ATRA and the miR-506-3p mimic synergistically promoted neuroblastoma cell differentiation.

After testing the response to ATRA in 15 neuroblastoma cell lines with neurite outgrowth assays, cell viability assays, and molecular differentiation markers, testing the response to miR-506-3p mimic in 5 neuroblastoma cell lines with neurite outgrowth assays, cell viability assays, and cell proliferation assays, and testing the combined treatment of ATRA and the miR-506-3p mimic on cell viability, the data provided here support the first hypotheses stated in Chapter I that the miR-506-3p mimic may have a more general effect on cell differentiation. The second hypothesis cannot be supported quantitatively by the data presented here, leaving more work to be performed for the combined treatments of ATRA and the miR-506-4p mimic on neuroblastoma cell lines to determine if the effect on cell viability is synergistic, additive, or antagonistic. The work here supports the hypothesis that the miR-506-3p mimic may have a broader effect than ATRA on neuroblastoma cell differentiation, and that an enhanced effect was observed (i.e., more cells died) for the combined treatment of ATRA and the miR-506-3p mimic.

To supplement the arguments presented in this study, more work is required. This includes testing the long-term effect of ATRA on cell proliferation in all 15 neuroblastoma cell lines, analyzing the response to the miR-506-3p mimic in the remaining 10 neuroblastoma cell lines using all four techniques (i.e., neurite outgrowth assay, cell viability assay, cell proliferation assay, and Western Blot), determining the statistical significance of the correlation between ATRA and the miR-506-3p mimic treatments (i.e., correlation analysis), and running the combined treatment experiments with reduced concentrations of the individual agents.

In conclusion, this data strongly indicates that miR-506-3p is a good candidate for a differentiation-inducing therapeutic agent for neuroblastoma, either alone or in combination with ATRA. The experiments here support this idea, but require more work and a deeper investigation into this process to further elucidate the problem of differentiation loss in neuroblastoma, and to develop new therapies and treatments for this disease.

REFERENCES

1. Park, J.R., Eggert, A., and Caron, H., (2010) Neuroblastoma: Biology, Prognosis, and Treatment, *Hematol Oncol Clin North Am 24*, 65-86.
2. Jemal, A., Siegel, R., Ward, R., Hao, Y., Xu, J., and Thun, M.J., (2009) Cancer Statistics, 2009, *CA: A Cancer Journal for Clinicians 59*, 225-249.
3. Neuroblastoma – Childhood – Statistics. (2012, June 25). Retrieved Devember 14, 2015, from http://www.cancer.net/cancer-types/neuroblastoma-childhood/statistics
4. Louis, C. U.; & Shohet, J. M. (2015). Neuroblastoma: Molecular Pathogenesis and Therapy. *Annual Review of Medicine 66*, 49–63.
5. Ngan, E.S. (2015) Heterogeneity of Neuroblastoma. *Oncoscience 2*, 837-838.
6. Knudson, A. G. (1971). Mutation and Cancer: Statistical Study of Retinoblastoma. *Proceedings of the National Academy of Sciences of the United States of America 68*, 820–823.
7. Nordling, C. O. (1953). A New Theory on the Cancer-inducing Mechanism. *British Journal of Cancer 7*, 68–72.
8. Zhao, Z., Ma, X., Hsiao, T.H., Lin, G., Kosti, A., Yu, X., Suresh, U., Chen, Y., Tomlinson, G.E., Pertsemlidis, A., and Du, L., (2014) A High-content Morphological Screen Identifies Novel MicroRNAs that Regulate Neuroblastoma Cell Differentiation, *Oncotarget 5*, 2499-2512.
9. Olynik, B.M., and Rastegar, M. (2012) The Genetic and Epigenetic Journey of Embryonic Stem Cells into Mature Neural Cells. *Frontiers in Genetics 3*, 81.
10. Maris, J.M., Hogarty, M.D., Bagatell, R., and Cohn, S.L., (2007) Neuroblastoma, *Lancet 369*, 2106-2120.
11. Brodeur, G.M.; and Bagatell, R. (2014) Mechanisms of Neuroblastoma Regression. *Nature Reviews. Clinical Oncology 11*, 704-713.
12. Brodeur, G. M.; Minturn, J. E.; Ho, R.; Simpson, A. M.; Iyer, R.; Varela, C. R.; and Evans, A. E. (2009). Trk Receptor Expression and Inhibition in Neuroblastomas. *Clinical Cancer Research : An Official Journal of the American Association for Cancer Research 15*, 3244–3250.
13. Thiele, C. J.; Li, Z.; & McKee, A. E. (2009). "On *Trk*" - the TrkB signal transduction pathway is an increasingly important target in cancer biology. *Clinical Cancer Research : An Official Journal of the American Association for Cancer Research 15*, 5962–5967.
14. Watson, J.D.; Baker, T.A.; Bell, S.P.; Gann, A.; Levine, M.; Losick, R.; and Harrison, S.C. (2013) Molecular Biology of the Gene (7^{th} ed.). Cold Spring Harbor, NY: Pearson, 242-249.

15. Hahn, C. K.; Ross, K. N.; Warrington, I. M.; Mazitschek, R.; Kanegai, C. M.; Wright, R. D.; Kung, A.L.; Golub, T.R.; and Stegmaier, K. (2008). Expression-based screening identifies the combination of histone deacetylase inhibitors and retinoids for neuroblastoma differentiation. *Proceedings of the National Academy of Sciences of the United States of America 105*, 9751–9756.
16. Cruz, F.D., and Matushansky, I., (2012) Solid Tumor Differentiation Therapy – is it possible?, *Oncotarget 3*, 559-567.
17. Ora, I., and Eggert, A. (2011) Progress in treatment and risk stratification of neuroblastoma: Impact on future clinical and basic research, *Seminars in Cancer Biology 21*, 217-228.
18. Carta, A., Chetcuti, R., and Ayers, D. (2014) An Introspective Update on the Influence of miRNA's in Breast Carcinoma and Neuroblastoma Chemoresistance. *Genetics Research International 2014*, 743050.
19. Stallings, R.L., Foley, N.H., Bray, I.M., Das, S., and Buckley, P.G. (2011) MicroRNA and DNA Methylation Alterations Mediating Retinoic Acid Induced Neuroblastoma Cell Differentiation. *Seminars in Cancer Biology 21*, 283-290.
20. Almeida, M.I.; Reis, R.M.; and Calin, G.A. (2011) MicroRNA History: Discovery, Recent Applications, and Next Frontiers. *Mutation Research 717*, 1-8.
21. Soriano, A., París-Coderch, L., Jubierre, L., Martínez, A., Zhou, X., Piskareva, O., Bray, I., Vidal, I., Almazán-Moga, A., Molist, C., Roma, J., Bayascas, J., Casanovas, O., Stallings, R., Toledo, J., Gallego, S., & Segura, M. (2016). MicroRNA-497 impairs the growth of chemoresistant neuroblastoma cells by targeting cell cycle, survival and vascular permeability genes. *Oncotarget 7*, 9271-9287.
22. Buhagiar, A., and Duncan Ayers (2015) Chemoresistance, Cancer Stem Cells, and miRNA Influences: The Case for Neuroblastoma, *Analytical Cellular Pathology* 2015, 8 pages.
23. Kisseljov, F.L. (2013) MicroRNA's and Cancer, *Molecular Biology* 48, 197-206.
24. Arora, A., Singh, S., Bhatt, A.N., Pandey, S., Sandhir, R., and Dwarakanath, B.S. (2015) Interplay Between Metabolism and Oncogenic Process: Role of microRNAs.*Translational Oncogenomics 7*, 11-27.
25. Calin, G.A., Dumitru, C.D., Shimizu, M., Bichi,R., Zupo, S., Noch, E., Aldler, H., Rattan, S., Keating, M., Rai, K., Rassenti, L., Kipps, T., Negrini, M., Bullrich, F., and Croce, C. (2002) Frequent deletions and down-regulation of micro- RNA genes *miR15* and *miR16* at 13q14 in chronic lymphocytic leukemia. *Proceedings of the National Academy of Sciences of the United States of America 99*, 15524-15529.
26. Verissimo, C.A.; Molennar, J.J.; Fitzsimmons, C.P.; and Vreugdenhil, E. (2011) Neuroblastoma Therapy: What is in the Pipeline? *Endocr Relat Cancer 18*, R213-R231.

27. Chen, Y., and Stallings, R.L. (2007) Differential Patterns of MicroRNA Expression in Neuroblastoma are correlated with Prognosis, Differentiation, and Apoptosis. *Cancer Research 67*, 976-983.
28. Zhao, Z., Ma, X., Hsiao, T.H., Lin, G., Kosti, A., Yu, X., Suresh, U., Chen, Y., Tomlinson, G.E., Pertsemlidis, A., and Du, L., (2014) A High-content Morphological Screen Identifies Novel MicroRNAs that Regulate Neuroblastoma Cell Differentiation, *Oncotarget 5*, 2499-2512.
29. Roth, SA; Knutsen, E.; Fiskaa, T.; Utnes, P.; Bhavsar, S.; Hald, O.H.; Løkke, C.; Mestdagh, P.; Johansen, S.D.; Flægstad, T.; and Einvik, C. (2016) Next generation sequencing of microRNAs from isogenic neuroblastoma cell lines isolated before and after treatment. *Cancer Letters 372*,128-136.
30. Samaraweera, L.; Grandinetti, K.B.; Huang, R.; Spengler, B.A.; and Ross, R.A. (2014) MicroRNAs define distinct human neuroblastoma cell phenotypes and regulate their differentiation and tumorigenicity. *BMC Cancer 14*, 2-11.
31. Welch, C.; Chen, Y.; and Stallings, R.L. (2007). MicroRNA-34a functions as a potential tumor suppressor by inducing apoptosis in neuroblastoma cells. *Oncogene 26*, 5017–5022.
32. Tivnan, A., Orr, W.S., Gubala, V., Nooney, R., Williams, D.E., McDonagh, C., Prenter, S., Harvey, H., Domingo-Fernandez, R., Bray, I.M., Piskareva, O., Ng, C.Y., Lode, H.N., Davidoff, A.M., and Stallings, R.L. (2012) Inhibition of Neuroblastoma Tumor Growth by Targeted Delivery of MicroRNA-34a Using Anti-Disialoganglioside GD_2 Coated Nanoparticles. *PLoS One 7*, e38129.
33. Yu, X.; Zhang, L.; Wen, G.; Zhao, H.; Luong, L. A.; Chen, Q.; Huang, Y.; Zhu, J.; Ye, S.; Xu, Q.; Wang, W.; and Xiao, Q. (2015). Upregulated sirtuin 1 by miRNA-34a is required for smooth muscle cell differentiation from pluripotent stem cells. *Cell Death and Differentiation 22*, 1170–1180.
34. Aranha, M. M., Santos, D. M., Solá, S., Steer, C. J., & Rodrigues, C. M. P. (2011). miR-34a Regulates Mouse Neural Stem Cell Differentiation. *PLoS ONE 6*, e21396.
35. Agostini, M.; Tucci, P.; Steinert, J. R.; Shalom-Feuerstein, R.; Rouleau, M.; Aberdam, D.; Forsythe, I.D.; Young, K.W.; Ventura, A.; Concepcion, C.P.; Han, Y.C.; Candi, E.; Knight, R.A.; Mak, T.W.; and Melino, G. (2011). MicroRNA-34a regulates neurite outgrowth, spinal morphology, and function. *Proceedings of the National Academy of Sciences of the United States of America 108*, 21099–21104.
36. Makeyev, E.V.; Zhang, J.; Carrasco, M.A.; and Maniatis, T. (2007). The MicroRNA miR-124 Promotes Neuronal Differentiation by Triggering Brain-Specific Alternative Pre-mRNA Splicing. *Molecular cell*. *3*, 435-448.

37. Mondanizadeh. M.; Arefian, E.; Mosayebi, G.; Saidijam, G.; Khansarinejad, B.; and Hashemi, S.M. (2015). MicroRNA-124 Regulates Neuronal Differentiation of Mesenchymal Stem Cells by Targeting Sp1 mRNA. Journal of Cellular Biochemistry 116, 943-953.
38. Åkerblom, M.; Sachdeva, R.; Barde, I.; Verp, S.; Gentner, B.; Trono, D.; and Jakobsson, J. (2012). MicroRNA-124 Is a Subventricular Zone Neuronal Fate Determinant. *The Journal of Neuroscience : The Official Journal of the Society for Neuroscience 32*, 8879–8889.
39. Zou, D., Chen, Y., Han, Y., Lv, C., & Tu, G. (2014). Overexpression of microRNA-124 promotes the neuronal differentiation of bone marrow-derived mesenchymal stem cells. *Neural Regeneration Research 9*, 1241–1248.
40. Dong, L.; Chen, L.; Wang, W.; and Zhang, L. (2015). Decreased expression of microRNA-124 is an independent unfavorable prognostic factor for patients with breast cancer. *Diagnostic Pathology 10*, 45.
41. Zhao, Z.; Ma, X.; Sung, D.; Li, M.; Kosti, A.; Lin, G.; Chen, Y.; Pertsemlidis, A.; Hsiao, T.H.; and Du, L. (2015). MicroRNA-449a functions as a tumor suppressor in neuroblastoma through inducing cell differentiation and cell cycle arrest. *RNA Biology 12*, 538–554.
42. Liu, T.; Hou, L.; Zhao, Y.; and Huang, Y. (2014). Epigenetic Silencing og HDAC1 by miR-449a upregulates Runx2 and promotes osteoblast differentiation. *International Journal of Molecular Medicine 35,* 238-246.
43. Capuano, M.; Iaffaldano, L.; Tinto, N.; Montanaro, D.; Capobianco, V.; Izzo, V.; Tucci, F.; Troncone, G.; Greco, L.; and Sacchetti, L. (2011). MicroRNA-449a Overexpression, Reduced NOTCH1 Signals and Scarce Goblet Cells Characterize the Small Intestine of Celiac Patients. *PLoS ONE 6,* e29094.
44. Foley, N.H., Bray, I., Watters, K.M., Das, S., Bryan, K., Bernas, T., Prehn, J.H., and Stallings, R.L. (2011) MicroRNAs 10a and 10b are potent inducers of neuroblastoma cell differentiation through targeting of nuclear receptor corepressor 2. *Cell Death Differ 18*, 1089–1098.
45. Li, J.; Zhang, Y.; Zhao, Q.; Wang, J.; and He, X. (2015). MicroRNA-10a influences osteoblast differentiation and angiogenesis by regulating β-Catenin expression. *Cellular Physiology and Biochemistry 37,* 2194-2208.
46. Zhi, F., Wang, R., Wang, Q., Xue, L., Deng, D., Wang, S., and Yang, Y. (2014) MicroRNAs in Neuroblastoma: Small-sized Players with a Large Impact. *Neurochemical Research 39*, 613-623.
47. Laneve, P.; Di Marcotullio, L.; Gioia, U.; Fiori, M. E.; Ferretti, E.; Gulino, A.; Bozzoni, I.; and Caffarelli, E. (2007). The interplay between microRNAs and the neurotrophin receptor tropomyosin-related kinase C controls proliferation of human neuroblastoma cells. *Proceedings of the National Academy of Sciences of the United States of America 19*, 7957–7962.

48. Foley, N.H.; Bray, I.M.; Tivnan, A.; Bryan, K.; Murphy, D.M.; Buckley, P.G.; Ryan, J.; O'Meara, A.; O'Sullivan, M.; and Stallings, R.L. (2010). MicroRNA-184 inhibits neuroblastoma cell survival through targeting the serine/threonine kinase AKT2. *Molecular Cancer 9*, 83.
49. Kos, A.; Olde Loohuis, N. F. M.; Wieczorek, M. L.; Glennon, J. C.; Martens, G. J. M.; Kolk, S. M.; and Aschrafi, A. (2012). A Potential Regulatory Role for Intronic microRNA-338-3p for Its Host Gene Encoding Apoptosis-Associated Tyrosine Kinase. *PLoS ONE 2*, e31022.
50. Masi, M.; Frolova, L.V.; Yu, X.; Mathieu, V.; Cimmino, A.; De Carvalho, A.; Kiss, R.; Rogelj, S.; Pertsemlidis, A.; Kornienko, A.; and Evidente, A. (2015). Jonqualine, a new pretazettine-type alkaloid isolated from *Narcissus jonquilla quail*, with activity against drug-resistant cancer. *Fitoterapia 102*, 41-48.
51. Bliss, C.I. (1939). The Toxicity of Poisons Applied Jointly1. *Ann Appl Biol 26*, 585-615.